Synthesis, experimental, theoretical study and molecular docking of 1-ethylpiperazine-1,4-diium bis(nitrate)

S. Gatfaoui, A. Sagaama, Noureddine Issaoui, T. Roisnel, Houda Marouani

AUTHOR CONTRIBUTION STATEMENTS

Sofian Gatfaoui: Formal analysis and Writing.

Abir Sagaama: Writing

Noureddine Issaoui : Software and Validation

Thierry Roisnel : Software

Houda Marouani : Supervision and Validation

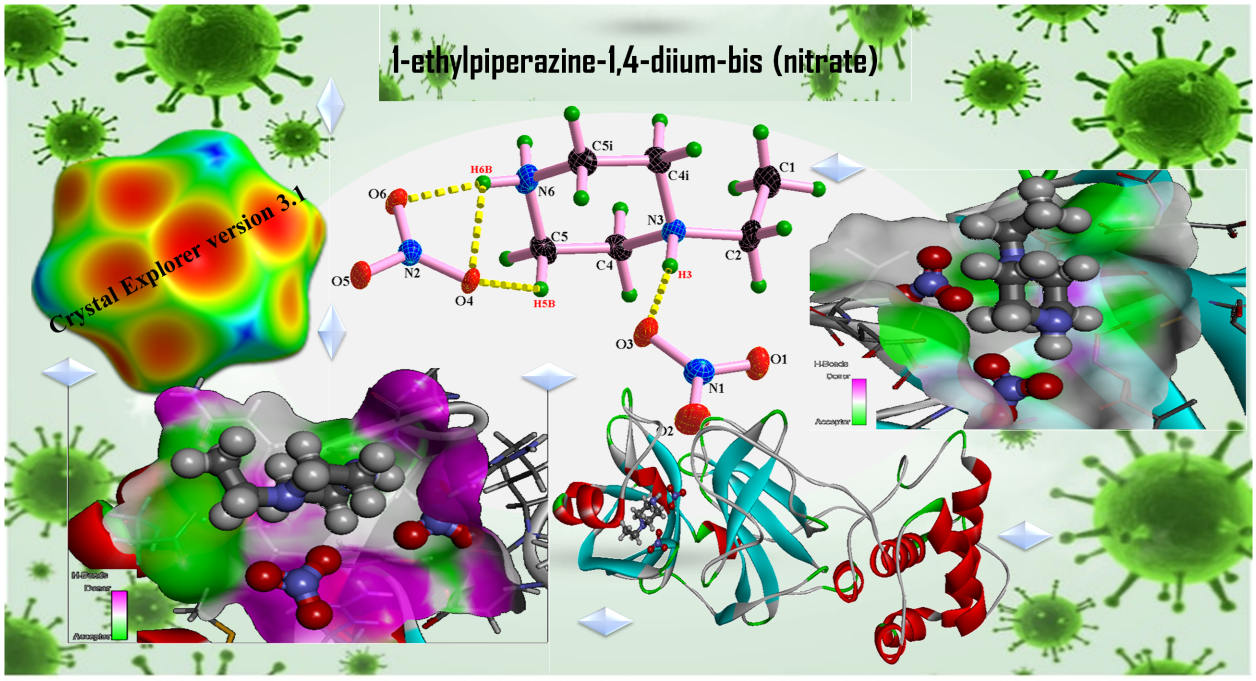

Synthesis, experimental, theoretical study and molecular docking of 1-ethylpiperazine-1,4-diium bis(nitrate)

Sofian Gatfaoui[(a)], Abir Sagaama[(b)], Noureddine Issaoui[(b)], Thierry Roisnel[(c)] and Houda Marouani[(a)*].

[(a)]Université de Carthage, Faculté des Sciences de Bizerte, LR13ES08 Laboratoire de Chimie des Matériaux, 7021, Bizerte,Tunisie
[(b)]University of Monastir, Laboratory of Quantum and Statistical Physics LR18ES18, Faculty of Sciences, Monastir 5079, Tunisia
[(c)]Univ Rennes, CNRS, ISCR (Institut des Sciences Chimiques de Rennes) – UMR 6226, F-35000 Rennes, France

*Correspondence e-mail: houdamarouani2015@gmail.com ; houda.marouani@fsb.rnu.tn

ABSTRACT

The present work undertakes the study of a new hybrid material $C_6H_{16}N_2(NO_3)_2$ symbolized as follows **1EPBN** (**1**-**E**thyl**p**iperazine-1,4-diium **B**is(**N**itrate)), a synergy between the two experimental and theoretical approach allows us to characterize and evaluate our crystal. **1EPBN** has been successfully synthesized at room temperature by slow evaporation and crystallized to the orthorhombic system with space group Pnma with a following lattice parameters are 12.158(2) Å, 6.5939(9) Å, 13.058(2) Å, V = 1046.8(3) $Å^3$ and Z = 4. The diprotonated 1-ethylpiperazine molecules are linked to the nitrate anions by multiple bifurcated and non-bifurcated N—H…(O,O) and weak C—H…O hydrogen bonds forming $R_1^4(4)$, $R_2^1(5)$, $R_2^1(6)$ and $R_4^2(10)$ motifs. The hydrogen bonding network is confirmed by the great contribution of O...H / H...O contacts (63.2%) on the Hirshfeld surface. Topological analysis such as atom in molecule (AIM), reduced density gradient (RDG) natural bond orbital (NBO), molecular electrostatic potential (MEP) and Mulliken charges have been used to evaluate in detail the intermolecular interactions, especially the hydrogen bonds. The HOMO and LUMO energies and other calculated quantum parameters reveal the hardness and the great stability of the material. Molecular docking analysis reveals that **1EPBN** might display the inhibitory activity against coronavirus proteins (COVID-19 and SARS-CoV2).

Keywords: X-ray diffraction, COVID-19, Molecular docking, NBO, HOMO-LUMO, Hirshfeld surface.

1. Introduction

Piperazine and its derivatives teach the family of nitrogen heterocycles consisting of a saturated six-atom ring containing two nitrogen atoms in opposite positions. In the broad

sense the combination of its organic compounds with other inorganic particles taking into account the pharmacological, biological, optical, thermal, electrical properties opens a wide field of application in various domain, namely in biology, photo-catalysis, medicine **[1-8]** ... Among its materials, nitrate compounds and their important properties are the subject of our work. First of all, it is very interesting to appreciate the pharmacokinetics and the mechanisms of action of the nitrate groups because when they are applied in pharmacies, as in the case of glyceryl trinitrate, their measurement of the plasma concentrations is very difficult, as mentions it Bogaert **[9]**, then one can quote for example the use of nitrates, in the systems of biological treatment or like pharmacological products **[10-14]**, they also penetrated the optoelectronics and nonlinear optics fields. Also organic nitrate possesses interesting antioxidant properties, this is demonstrated by the scavenging of DPPH radicals, of ABTS radicals, the reduction of properties and a slight trapping of hydroxyl radicals to that of ascorbic acid **[15,16]**. More particularly, this study includes the synthesis and characterization of the new hybrid material 1-ethylpiperazine-1,4-diium bis(nitrate) (**1EPBN**) using single crystal X-ray diffraction and quantum chemical methods. Hirshfeld surface and fingerprints plots calculations evaluated and confirmed the results observed by X-ray diffraction. The AIM, RDG, NBO approaches have been widely applied to classify and understand the hydrogen bonding interactions in the prepared material. MEP descriptor was made to predict reactive sites within the crystal. The HOMO-LUMO gap energy is calculated and other electronic properties are then deduced. Molecular docking analysis is very convenient tool for the investigation of biological activities of the studied compound. In this context various docking studies have been mentioned in drug design **[17-22]**. In this paper, molecular docking study was made to examine the inhibition mechanism of our molecule with the novel corona virus disease.

2. Experimental

2.1 Materials and measurements

The 1EPBN single crystal is chosen according to its size 0.13 x 0.30 x 0.54 mm and its morphology, it must be a regular shape (prismatic) for studies by X-ray diffraction. Data collection is carried out on a diffractometer automatic D8 VENTURE Bruker-AXS with four circles and detector CCD type consists of a sealed tube generator (3 kW in fine hearth with anticathode in MoKα, (λ = 0.71073 Å) at 150 K). Absorption corrections were performed using the multi-scan technique using the SADABS program **[23]**. The total number of measured reflections was 6291 ($3.1° < \theta < 27.5°$) among which 1297 were independent and 1185 had intensity $I > 2\sigma$ (I). The crystal structure of the compound was resolved by direct

methods using the SIR97 program **[24]** and then refined by the least-square methods coupled with Fourier synthesis using the SHELXL-97 program **[25]** implemented in the WINGX software **[26]** to $R_1(F^2)$ = 0.035, $wR_2(F^2)$ = 0.096. All non-hydrogen atoms were refined with anisotropic atomic displacement parameters. The hydrogen atoms bonded to nitrogen atoms were located from a difference map. The rest of the H atoms were treated by a mixture of independent and constrained refinement. Structure graphics are drawn with ORTEP **[26]** and Diamond program **[27].**

2.2. Theoretical studies

Hirshfeld surface analysis is based on a 3D graph that represents the space region where the molecules come in contact and another 2D that summarizes the complexes information contained in a structure and makes it possible to identify each type of interaction. This analysis was performed using the Crystal Explorer software **[28].**

The geometrical optimization of 1EPBN carried out by the quantum chemistry methods and especially the DFT method (Density Functional Theory) implemented in the Gaussian program 09 **[29]** using the functional hybrid B3LYP (Becke's three parameter exchange functional B3 combined with Lee-Yang-Parr correlation functional BLYP) / 6-311++G(d,p) **[30-31]**. The pictorial evidence for the intermolecular interactions collected from the topological proprieties were performed using Multiwfn multifunctional wave function analyzer **[32]** and plotted using VMD molecular visualization program [33]. In this study, NBO calculations **[34]** were employed to determinate the energy of intermolecular interactions, Molecular docking calculations of ligand-proteins complex are carried out via iGEMDOCK **[35]** based on GEMDOCK scoring function. The intermolecular interactions were plotted using Discovery studio visualizer **[36]** interface.

2.3 Synthesis of $C_6H_{16}N_2(NO_3)_2$

The compound is prepared by adding dropwise a quantity of nitric acid (1mmol) diluted in 10 mL of distilled water to an ethanolic solution (10mL) containing 1mmol of 1-ethylpiperzine with magnetic stirring. The solution obtained is subjected to slow evaporation at room temperature. After one week, transparent, prismatic, stable monocrystals are formed, of suitable size for study by X-ray diffraction.

The diagram of the chemical reaction from which the crystals come is:

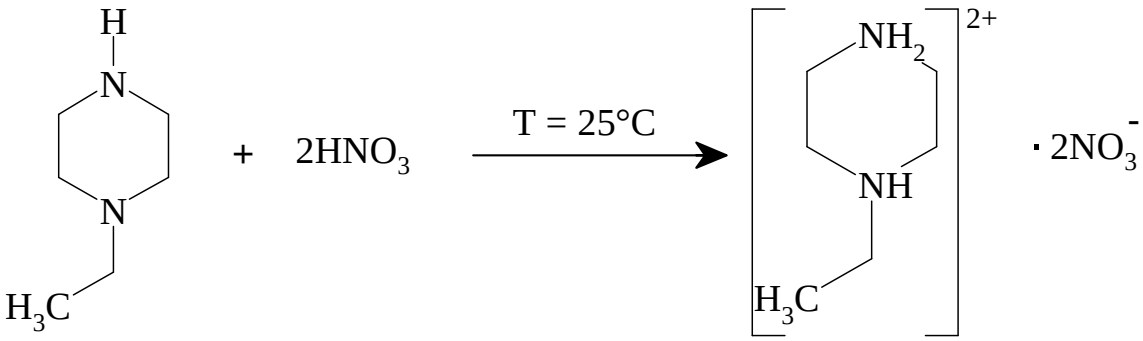

3. Results and discussion

3.1. X-ray diffraction

After having synthesized the 1EPBN material we studied it by X-ray diffraction, it is the main technique that we used to determine in a first step the conditions of the collection, of data processing and the results of the structural resolution of our structure which are recorded in Table 1 and in a second step their atomic arrangement. Fig. 1 is an ORTEP representation of the structure of $C_6H_{16}N_2(NO_3)_2$ containing two nitrate anions (NO_3^-), and an organic cation 1-ethylpiperazine-1,4-diium ($C_6H_{16}N_2^{2+}$) . The projections of this structure along the $\vec{a}$ and $\vec{b}$ directions which are given respectively in Fig. 2 show the atomic organization of chemical buildings involved in the composition of the crystal in the form of the infinite layers located in y = 1/4 and y = 3/4 position parallel to (ac) plane. Indeed the diprotonated cations 1-ethylpiperazine is grafted to the anions (NO_3^-) by establishment of the bifurcated and non-bifurcated hydrogen bonds N−H… O (O, O) and C−H… O (O, O) (Fig. 3) forming a three-dimensional network. This hydrogen bonding network generates various types of pore, namely R_1^2 (4), R_2^1 (5) and R_2^1 (6) formed by two entities (NO_3^- and $C_6H_{16}N_2^{2+}$) and R_4^2 (10) made up of four alternating entities ($2NO_3^-$ and $2C_6H_{16}N_2^{2+}$). The values of the interatomic distances (N − O) and bond angles (O − N − O) describing the local geometry of the inorganic group NO_3^- reported in Table 2 vary from 1.2407 (15) to 1.2665 (16) Å and from 119.26 (12) to 121.24 (13) ° respectively, these values are in good agreement with those observed in other similar nitrate **[37-41]**. Comparing the N1 − O1, N1 − O2 and N2 − O4 distances with those N1 − O3, N2 − O5 and N2 − O6 we observe that the latter are very long compared to others, because the O3, O5 and O6 atoms are involved in strong hydrogen bonds (Table 3). Concerning the cationic part, the diprotonation of 1-ethylpiperazine ($C_6H_{14}N_2$), according to the experimental protocol leads to the 1-ethylpiperazine-1,4-diium ($C_6H_{16}N_2^{2+}$) cations positively charged to neutralize the anions of the anionic part. The distances and angles describing the latter are shown in Table 2. The piperazinium cycle adopts a substituted geometry by an ethyl group ($-CH_2-CH_3$) in position N3 with interatomic distances C1 − C2

and C2 − N3 respectively equal 1.522 (2) and 1.5074 (17) Å. In the piperazinium cycle the distances made between the N3 − C4, C4 − C5 and C5 − N6 atoms have an average value equal to 1.50 Å. On the other hand, the values of the C-C-N and C-N-C angles vary from 109.72 (10) to 113.77 (11)°. These distances and these connection angles do not significantly differences from those encountered in several materials containing organic cations based on piperazine **[15, 41, 42]**. In the **1EPBN** structure the organic matrix comprises two types of N − H and C − H donors located at the level of the piperazinium cycle. The oxygen atom O3 of the nitrate anion $(N1O_3)^-$ engaged in a single hydrogen bond N3 − H3… O3 with a donor-acceptor distance N3… O3 equal to 2.7757 (16) Å, the three oxygen atoms (O4, O5, and O6) of the nitrate anion $(N2O_3)^-$ are engaged in six hydrogen bonds including four C − H… O and one N − H… O where the donor-acceptor distances ranging from 3.0982 (16) to 3.4726 (13) Å. The strength of its hydrogen bonds can be interpreted according to the Brown and Blessing [43-44] criteria of relating to the donor-acceptor distances (D… A). Indeed, if:

* d (D… A) > 2.73Å the hydrogen bond is considered to be weak.

* d (D… A) < 2.73Å the hydrogen bond is considered to be strong.

So the hydrogen bonds existing in our compound **1EPBN**, according to these criteria are classified weak. We conclude that the synergy of the hydrogen bond network, the van der Waals interactions and the electrostatic interactions contribute a lot to the stability and cohesion of the crystal structure.

Note that our 1EPBN structure is very similar to the 1-methylpiperazine-1,4-diium bis(nitrate) structure **[15]**, they crystallize in the same orthorhombic system having the same group space Pnma, even if at level of the mesh parameters these two structures do not present a remarkable difference, also the ionic entities have mirror planes crossing the nitrate anions and the ethyl/methyl and ammonium groups of the piperazine cycle. So we can say that changing $(-CH_3)$ by $(-CH_2-CH_3)$ do not influence much point of view differentiability at level of the two structures.

3.2. Geometric optimization

A comparative study was carried out using the results of the experimental study by X-ray diffraction and the results of the conformational study obtained by the DFT method according to the B3LYP hybrid method with the calculation base 6-311++G(d,p). The geometric parameters obtained from these calculations correspond to the most stable geometry for the 1EPBN molecule are listed as follows, energy (-908.654026 Hartree), dipole moment (9.758524 Debye), polarizability (137.414540 a.u.) and hyperpolarisability

(351.414540 a.u.). We illustrate in the Fig. 4 the optimized geometrical structure of 1EPBN, the structural parameters such as the interatomic distances and the connection angles relative to this optimization are recorded in the Table 2. The interatomic distances (N − O) and the angles connection (O − N − O calculated respectively vary from 1.2024 to 1.3722 Å and 115.3746 to 127.7517 °. Inspection of this table shows that calculated values at B3LYP level are in good agreement with the experimental values and do not have any particular characteristic, they are comparable to those encountered in other similar structures **[45, 46]**. Concerning the organic part of the studied crystal the values of C − N and C − C bonds calculated theoretically by the DFT method ranging from 1.4764 to 1.5324 Å while the angles lie in the [110.6102 ° - 117.2938 °] interval. The error does not exceed 3% for the links and 2% for the angles. So the gap is relatively small between the values of the experimental and theoretical approaches. These differences are probably due to the fact that in theoretical calculation, an isolated molecule is considered in gas phase while in the experimental measurement the molecules are in condensed phase. Therefore as it has been discussed in the literature, it is well known that B3LYP method predicts geometric parameters, which are much closer to experimental data.

3.3 3D normalized distance and 2D fingerprints plots

Figures 5a, 5c are a typical example of the images obtained by considering d_{norm} mapping as a mode of representation of the Hirshfeld surface of the molecule analyzed. A color gradient is used to quantify the interactions taking place between atoms within the studied crystal, this gradient varies from blue to red through white. By considering inter and intramolecular interactions, the bluish domains indicate that the distance separating neighboring atoms exceeds the sum of their respective van der Waals rays. The white areas mark the places where the distance between neighboring atoms is close to the sum of the van der Waals radius of considered atoms. The color red is used to represent the places where there is interpenetration of van der Waals rays from neighboring atoms. A quantitative representation as a percentage function summarizes all the intermolecular contacts existing in the 1EPBN structure is shown in Fig. 6. The study of the d_{norm} mapping of 1EPBN represented in (Fig. 5a) makes it possible to highlight contacts taking place between certain hydrogen atoms ($RVW_{\mathbf{H}}$ = 1.09 Å) located in the *para* and *meta* position and oxygen atoms ($RVW_{\mathbf{O}}$ = 1.52 Å) which are attributed to N-H… O type hydrogen bonds displayed by large red spots and other C-H… O interactions weaker than N-H… O indicated by small red spots. The measured H… O distances, which range from 1.778 to 2.330 Å, are much less than the sum of

the van der Waals rays of these atoms (2.61 Å), this result also confirmed by the two-dimensional fingerprint recorded in (Fig. 5b) where it shows the majority of O… H / H… O contacts with a significant contribution to the Hirshfeld area equal to 63.2 %. These contacts represented by two narrow and symmetrical pointed points with a sum $d_e + d_i \sim 1.8$ Å less than the sum of the van der Waals rays of the involved atoms (H, O). A d_{norm} view of the 1-ethylpiperazine- 1,4-diium cation as depicted in Figure. 5c allows to visualize the contacts taking place between hydrogen atoms (H ... H), these inter contacts are located on blue and white regions of the d_{norm} mapping. The distances between the hydrogen atoms (H… H) varying from 2.343 to 2.489 Å, these magnitudes are greater than the sum of the van der Waals radii of the considered atoms which is 2.18 Å. The graph (2D) relating to these contacts is illustrated in Fig. 5d. The hydrogen-hydrogen intercontacts comprise 27.9% of the entire Hirshfeld surface around a maximum sum $d_e + d_i \sim 2.8$ Å greater than the sum of the van der Waals radii of the hydrogen atoms (2.18 Å). From this comparison it is concluded that only the hydrogen-oxygen contacts (H… O / O… H) attributable to the hydrogen bonds N-H… O and C-H… O are classified close together. Concerning the rest of the other contacts such as N… O / O… N (4%), O… O (3%), N… H / H… N (1.4%) and N… N (0.5%) has a very weak contribution on the Hirshfeld surface. The distances between the interacting atoms with each other for its contacts are greater than the sum of the van der Waals radii of the considered atoms, this allows us to classify them with the inter contacts H ... H among the distant contacts in the compound 1EPBN.

3.4 Quantum theory of atoms in molecules (QTAIMs) analysis

Many theoretical studies have shown that one of the most useful tools for characterizing atomic and molecular interactions, mainly hydrogen bonds, is topological analysis (AIM) **[47]**. According to this approach, each chemical bond has a critical point of bond, denoted "BCP". At this point, several topological parameters can be calculated, namely the electronic density ρ (r) and the Laplacian $\nabla^2\rho(r)$ (the Laplacian of electronic density is defined as the sum of the three eigenvalues of Hessian (λ1, λ2 and λ3)), the kinetic energy density (G), the potential energy density (V), the total energy density (H) with H = G + V and the binding energy (E_{bond} = V (r) / 2) **[48]**. These quantities have been used to evaluate the properties of bonds in the studied compound, especially the hydrogen bonds. Indeed, according to the results found in references **[49-52]**, a hydrogen bond exists if ρ(r), at the critical point, lies in 0.0020─0.0600 a.u. range, while $\nabla^2\rho(r)$ should be positive and located in 0,0240─0,150 a.u. region. On the basis of Rozas et al **[53]** criterion we have classified the hydrogen bonds in three categories:

- If $\nabla^2\rho(r) < 0$ and H (r) < 0: hydrogen bond considered strong.
- If $\nabla^2\rho(r) > 0$ and H (r) < 0: hydrogen bond considered average.
- If $\nabla^2\rho(r) > 0$ and H (r) > 0: hydrogen bond considered weak.

In addition AIM analysis allows us to detect the presence of cycles in a molecular system. The presence of a critical point in the "RCP" cycle confirms the cyclic nature of certain molecules and an atomic chain. The graphical representation of atom in molecule analysis (AIM) of the **1EPBN** compound is mapped in Fig. 7 while the corresponding topological parameters are grouped in Table 4. We can see from this table that at the BCPs located at O… H links, the electronic densities equal to 0.0065, 0.0327, 0.0084, 0.0084 and 0.0297 a.u. as well as the $\nabla^2\rho(r)$ values equal to 0.0249, 0.1085, 0.0279, 0.0279 and 0.0952 a.u. ($\nabla^2\rho(r) > 0$ detects depletion of electronic charge along the path of O… H links). We note that these values suggest existence of various hydrogen bonds such as C4-H5… O26, N6-H7… O28, C11-H13-O30, C22-H24… O30 and N14-H16… O32 having energy densities total (H) greater than zero, therefore according to Rozas et al **[53]** they can be classified in the range of weak hydrogen bonds; also this is confirmed by the bond energy $E_{H...O}$ values varying from -0.0129 to -0.0020 kJ.mol^{-1}. The AIM analysis also shows the existence of a critical point RCP at the piperazinium cycle and three new critical points NRCP1, NRCP2 and NRCP3 formed by hydrogen bonds which connect two nitrate anions (N25, N29) to the 1- ethylpiperazine-1,4-diium group. Indeed that the electronic density ρ(r) and of the Laplacian $\nabla^2\rho(r)$ at the RCP (0.0193, 0.1209 a.u.) point are higher than those located at NRCP1 (0.0060, 0.0249 a.u.), NRCP2 (0.0073, 0.0301 a.u.) and NRCP3 (0.0073, 0.0301 a.u.) points. This comparison clearly reveals the high stability of the piperazinium nucleus.

3.5 Reduced Density Gradient (RDG) and Isosurface Analysis

Besides experimental interpretations based on X-ray diffraction and other empirical studies such as Hirshfeld surfaces analysis and QTAIMs Johnson et al **[54]** proposed a new approach, the so-called RDG analysis to validate and evaluate the intermolecular interactions existing in the crystal structure of **1EPBN**. The RDG is a fundamental dimensionless quantity coming from the density and its first derivative:

$$RDG(r) = \frac{1}{2(3\pi^2)^{1/3}} \frac{|\nabla\rho(r)|}{\rho(r)^{4/3}}$$

Generally, according to the sign of the eigenvalue λ_2, we can determine of the stabilizing or destabilizing nature of the different interactions in **1EPBN** compound. The negative sign of λ_2 provides information on the interesting contributions to non-covalent interactions and more

specifically to hydrogen bonds, on the other hand the region where the sign $\lambda_2 > 0$ relates to repulsive and non-binding interactions (steric effect in ring and cage), the values located in the vicinity of the separation (close to zero) are attributed to the van der Waals interactions. The different plots and results obtained along this theoretical analysis according to a very precise color code are produced respectively using the Multiwfn and VMD programs and illustrated in Fig. 8a, 8b. The RDG fingerprint (Fig. 8a) shows the great stability of **1EPBN** ensured by strong hydrogen bonds N-H ... O and even if weak of the C-H ... O type. These obligations appeared with a sign $\lambda_2 \rho$ ranging from -0.015 to -0.005 Å. Also the isosurface representation (Fig. 8b) clearly indicates the presence of blue spots between the hydrogen and oxygen atoms, which signifies the strong attractive interaction N-H…O. The light intensity of the green color in the RDG isosurface proves the presence of a strong VDW interaction. Finally the elliptical red spot centered at the level of the piperazinium nucleus is attributed to repulsive interactions which show a strong steric effect.

3.6 Frontier molecular orbital insight

The spatial distribution of molecular orbital's, especially border orbits: the highest energy occupied molecular orbital HOMO (Highest Occupied Molecular Orbital) and the lowest energy unoccupied orbital LUMO (Lowest Unoccupied Molecular Orbital), are excellent indicators of electron transfer in molecular systems. These orbital's are largely involved in the chemical stability of the molecule and play an important role in determining its electronic properties. Indeed the two bands, valence band (LUMO) and conduction band (HOMO) are energetically separated by energy (E_{LUMO}-E_{HOMO}) called gap energy. This energy quantity is used to characterize the chemical reactivity and the kinetic stability of the molecule, hence if the HOMO-LUMO energy gap is high; the flow of electrons in the higher energy state is difficult, which makes the molecule more stable and less reactive. On the other hand, if the lower HOMO-LUMO energy gap is a criterion of high reactivity for the molecule. The values of the HOMO and LUMO orbital's and their energy difference (the gap (ΔE)) obtained by DFT with the functional B3LYP using the 6-311++G(d,p) shown in Fig. 9a. According to this figure the energy difference ΔE is close to 5.6997 eV in the gas phase (ΔE = 4.8675 eV in water), it can be said that it is a high value implies a high kinetic stability, a low chemical reactivity towards chemical reactions in a certain direction.

In addition to the energy gap, hardness and chemical softness are also good indicators of the chemical stability of a molecule. All the values previously mentioned and other quantum parameters such as electronic affinity (A), ionization potential (I), chemical potential (μ) and electronegativity (χ) and electrophelicity (Ψ) are calculated using the DFT method

B3LYP / 6-311++G(d,p), presented in Table 5 and mapped in Fig. 9b. These different parameters are defined by the following relationships:

- $I = -E_{HOMO}$
- $A = -E_{LUMO}$
- $\chi = \frac{I+A}{2}$ (defined by Mulliken **[55]**)
- $\eta = \frac{I-A}{2}$ (A hard molecule has a large gap energy **[56]**)
- $S = \frac{1}{\eta}$ (A soft molecule has a low gap energy **[56]**)
- $\Psi = \frac{\boldsymbol{\mu}^2}{2\eta}$ (A good nucleophile is characterized by weak ψ, and vice versa defined by Parr and al **[57]**)
- $\mu = -\frac{I+A}{2}$

We conclude it should be noted that the 1EPBN compound has a large ionization energy which is of the order of 7.6659 eV in gas phase and 7.1193 eV in water this confirms the great stability of our crystal. Concerning the hardness and chemical softness they are equal respectively 2.8498 and 1.4249 eV in gas phase, the large gap energy value suggests the hardness of the material (1EPBN). Closing by the very high electrophily index which is around 4.0693 eV (in gas phase) and 4.5108 eV (in water), this important quantity, classified our compound as being a good electrophile. Generally, the values of all these parameters have no particularity with respect to the values usually encountered in compounds based on nitrate **[16, 46]**.

3.7 Molecular electrostatic potential and Mullikan charges analysis

Knowing the charge distribution of a material allows us to obtain its electrostatic properties theoretically. For this, the electrostatic potentials V(r) of the optimized molecules have been calculated at level B3LYP / 6-31++G (d,p), using Gaussian programs. The map of electrostatic potential of the **1EPBN** compound is illustrated in Fig. 10a. Often this diagram is simply very useful for determining the electrophilic and nucleophilic sites as well as hydrogen bonding interactions **[58-59]**. The resulting model presents the regions of positive, negative and neutral electrostatic potential in terms of color gradation where the blue color indicates the strong attraction while the red presents a region of strong repulsion and the green indicates the neutral zone. Indeed, according to Fig. 10a, the red surfaces of the negative potentials are associated with the free doublets of the oxygen atoms come from the nitrate groups accepting the H^+ proton, on the other hand the blue zones of the positive potentials are attributed to the

two ammonium groups of the 1-ethylpiperazine-1,4-diium cation. Also in the same figure the electrophilic site (deficient in electrons) is observed (dark blue) at the level of hydrogen atoms of the organic cation. Whereas, the nucleophilic site (excess in electrons) is observed (dark red) at the level of oxygen atoms linked to the NO_3^- anions.

Mulliken's analysis is the analysis of the charges distribution on atoms in terms of population of molecular orbitals, plays a very important role in the application of calculations in quantum mechanics for molecular systems **[60]** it suggests the formation donor-acceptor pair, which involves the charges transfer in the molecule. The charge distributions calculated by the methods of Mulliken **[61]** and NBO, for the 1EPBN molecule, were carried out using the DFT / B3LYP method at the base level 6-311++G(d, p) and are presented in Table 6. These results are even better represented in a graphical form indicated in Fig. 10b. The charge distribution applied in the 1EPBN compound shows that all the carbon and nitrogen atoms carry negative charges, the atomic charges for the oxygen atoms were found to be both positive and negative ranging from -0.058477 to 0.044233, while all the hydrogen atoms having positive charges including two higher located on the H7 and H16 atoms, let us also note that nitrogen atoms N6 and N14 of the cationic group have two very weak charges which are respectively of the order -0.373457 and -0.407403. These results suggest the formation of intermolecular interactions and consequently promote the formation of hydrogen bonds such as N6-H7… O28 and N-14… H16.

3.8 Molecular docking investigation

In order to understand the binding interactions among ligand and its protein, molecular docking analysis is an excellent tool in drug design industry. As mentioned above, molecular docking calculations were reported throughout iGEMDOCK software. During computation, this program gives 10 poses and identifies the best pose associating with the weaker energy. In the current work, the intermolecular interactions were investigated for the title compound with two types of coronavirus; COVID-19 (6W63) **[62]** and SARS-CoV2 (6W4B) **[63]** which obtained from Protein Data Bank **[64]**. Molecular docking results of the compound with coronavirus proteins are tabulated in Table 7. The total energies (E_{int}) are -84.32 and -68.15 kcal/mol for COVID-19 and SARS-CoV2, respectively. As clearly seen from Table 1, the interaction energies are principally of type hydrogen bond (H-bond) and van der Waals (VDW). The results prove that the hydrogen bonding energy values in both complexes are stronger than VDW interactions values. The H-bond energy is founded to be -51.59 kcal/mol for 6W63-1EPBN and -37.85 kcal/mol for 6W4B-1EPBN complex. Whereas, the VDW energy values are -34.54 and -29.45 kcal/mol for COVID-19 and SARS-CoV2 proteins,

respectively. The corresponding docking position for 6W63 and 6W4B of 1EPBN are mapped in Fig. 11. However, the electronic acceptor-donor interactions were responsible to the formations of the hydrogen bonding interactions. As it is shown in Fig. 12, in both complexes the nitrate molecules (N_2O_6) in hydrogen bond participate as an electron donor, whereas the piperazine ring plays the role of an electron acceptor. Based in the color intensity of electron donor (pink color) and electron acceptor (green color), the H-bond interactions in 6W63-1EPBN are stronger than that in 6W4B-1EPBN.

As clearly seen in Fig. 13, the dotted lines represent the inter and intramolecular interactions in both complexes. The green lines characterize the hydrogen bond (H-bond), the yellow correspond to electrostatic interaction and the light blue color represents the carbon hydrogen bond (C-H…O). For 63W63-1EPBN interaction, the molecule interact with A:ARG:40, A:ARG:188, Z:PRE:999 and A:ASP:187 amino acid residues that implicated in H-bond, including bond lengths 4.6, 1.47, 1.78 and 2.54 Å. While, Z:PRE:999 participate with O26 (2.92 Å), H20 (1.81 Å), O28 (2.68 Å) and O30 (2.53 Å) forming carbon hydrogen bonds (C-H…O). In addition, A:ARG:40, A:ARG:188 and Z:PRE:999 residues are involved in electrostatic bond with distance value ranging from 1.89 to 5.57 Å. Concerning 63W63-1-EPN complex, B:LYS:87 and Z:PRE:999 are involved in electrostatic bond with bond lengths 2.71 Å (O31), 3.10 Å (O32), 3.51 Å (N25) and 4.62 Å (O28). In this system, there are five carbon hydrogen bonds resulted by the interactions of Z:PRE:999 amino acid residue with O28, O32, O26, N25, O28 and O30. Beside the B:SER:47 formed an H-bond interaction with oxygen atom O27 (2.58 Å). Comparing interactions in the systems, we can deduce that our molecule interact better with COVID-19 than with SARS-CoV2 viral proteins.

Based on molecular docking results, the interaction among 6W63 and 1EPBN ligand reveals the great inhibitor capacity of the working compound, demonstrating the promoter inhibitory effect in the treatment of the novel coronavirus.

3.9 Natural bond orbital investigation

NBO (Natural bond orbital) analysis plays a very important role in the interpretation of hyper-conjugate interactions and the transfer of electrons from free electron pairs LP(A) to the anti-binding orbital σ*(DH) of the hydrogen bond D─H…A. A perturbative analysis of the “donor-acceptor” interactions, called “second order perturbative analysis” is carried out between the occupied and vacant NBO. Consequently the second order stabilization energy $E^{(2)}$ associated with the delocalization of electrons between the donor and the acceptor is **[65]**:

$$E^{(2)} = \Delta E_{ij} = \frac{q_i F(i, j)}{\varepsilon_i - \varepsilon_j}$$

Where q_i is the occupation of orbital i. ε_i and ε_j are the diagonal elements (energies of orbitals i and j). F (i, j) is the Fock matrix element outside of the diagonal.

NBO analysis of the 1PBN compound was carried out and the corresponding results are tabulated in Table 8. The energy $E^{(2)}$ associated with the hyperconjugation of the LP1 (N6) → σ* (H7─O28) and LP1 (N14) → σ* (H16─O32) interactions, respectively is of the order of 40.01 and 44.48 kJ.mol^{-1}. These two important values result from the formation of the hydrogen bonds N−H…O which ensures the cohesion and the stability of the crystal edifice of 1EPBN material. The intermolecular interactions of LP(1)N6 → σ*(C1-C4), LP(1)N6 → σ*(C8-H10),LP(1)N6 → σ*(C19-H21), LP(1)N14 → σ*(C8-C11) and LP(1)N14 → σ*(C19-C22) leads to large stabilization of 5.74, 6.41, 6.30, 5.25 and 5.17 kJ.mol^{-1}. Other interactions are observed at the nitrate anions such as LP(3)O30 to σ(N29-O31), LP(2)O31 to σ*(N29-O30), LP(2)O31 to σ*(N29-O32), LP(2)O32 to σ*(N29-O31), LP(2)O30 to σ*(N29-O32), LP(2)O27 to σ*(N25-O26), LP(2)O27 to σ*(N25 -O28), LP(2) O28 to σ*(N25-O27), LP(2)O26 to σ*(N25-O28) and LP(3)O26 to σ*(N25-O27) which give, respectively, significant stabilization energies of 152.02, 17.13, 29.27, 40.13, 26.03, 17.36, 29.35, 39.67, 25.49 and 144.83 kJ.mol^{-1}. Indeed, the two large stabilization energies (152.02 and 144.83) attributed to the LP (3)O30 → σ*(N29-O31) and LP(3)O26 → σ*(N25-O27) interactions are explained by the absence of hydrogen bonds involved with O30, O3, O25 and O27 atoms. So the NBO analysis confirms well the sequence and organization of the network of hydrogen bonds already observed experimentally by X-ray diffraction and by other topological theoretical models namely the Hirshfeld surfaces analysis, AIM, RDG at the level of 1EPBN structure.

4. Conclusions

During this work, we synthesized the crystal structure of the 1-ethylpiperazine-1,4-diium bis(nitrate) (1EPBN) compound of chemical formula $C_6H_{16}N_2(NO_3)_2$, using, on the one hand, the experimental technique by X-ray diffraction and on the other hand, theoretical calculations of quantum chemistry to support the experimental results. The structural study shows that 1EPBN crystallizes in the orthorhombic crystal system (Pnma) and has a molecular arrangement whose cohesion and stability are ensured by a three-dimensional network of hydrogen bonds N-H ... O and C-H ... O. These bands have been confirmed and quantified by

Hirshfeld surfaces analysis; this analysis proves that the most important contacts are the O… H / H… O and H… H interactions type which contribute respectively with percentages of 63.2% and 27.9%. The theoretical method DFT B3LYP / 6-31++G(d, p) was used to have the geometric optimization; the results obtained by this method are compatible with those found by X-ray diffraction. AIM and RDG topological analyses have been reported to study the properties of hydrogen bonds in the title compound. The MEP (Molecular Electronic Potential) map shows that negative potential sites are located on the oxygen atoms of the nitrate groups, while the positive potential sites are located around the ammonium groups of 1-ethylpiperazine-1,4-diium cation. NBO orbital analysis has been used to study electronic exchanges, transfer reactions between donor-acceptor compounds and hyperconjugation interactions. The frontier molecule provides orbital information about HOMO-LUMO energy gap, ionization potential, electronic affinity, hardness and other chemical descriptors. In the same context of molecular modeling, we have studied the molecular docking of our structure; it is used as a guide to identify a preferential orientation of a ligand in the receptor. This molecular model suggests that 1EPBN molecule interacts better with COVID-19 than with viral proteins SARS-CoV2, also demonstrating the inhibitory effect of promoter in treatment of the new coronavirus.

Acknowledgements

We are grateful to the Tunisian Ministry of Higher Education Scientific Research for the provided financial support.

REFERENCES

[1] P. Englebienne, A.V. Hoonacker, Goldeconductive polymer nanoparticles: a hybrid material with enhanced photonic reactivity to environmental stimuli, J. Colloid Interface Sci. 292 (2) (2005) 445-454.

[2] A. Müller, H. Reuter, S. Dillinger, Supramolecular inorganic chemistry: small guests in small and large hosts, Angew. Chem. Int. Ed. Engl. 34 (1995) 2328-2361.

[3] Y. Li, Y. Yu, L. Wu, J. Zhi, Processable polyaniline/titania nanocomposites with good photocatalytic and conductivity properties prepared via peroxotitanium complex catalyzed emulsion polymerization approach, Appl. Surf. Sci. 273 (2013) 135-143.

[4] G.K. Gribble, M.G. Saulnier, M.P. Sibi, J.A. Obaza-Nutaitis, Synthesis and dielsalder reactions of 1,3-dimethyl-4-(phenylsulfonyl)-4H-furo[3,4-b]indole. A new annulation strategy for the construction of ellipticine and isoellipticine, J. Org. Chem. 49 (1984) 4518 -4523.

[5] A. Müller, F. Peters, M.T. Pope, D. Gatteschi, Polyoxometalates: very large clusters-nanoscale magnets, Chem. Rev. 98 (1998) 239-272.

[6] L.M. Novena, S.S. Kumar, S. Athimoolam, Improved solubility and bioactivity oftheophylline (a bronchodilator drug) through its new nitrate salt analysed by experimental and theoretical approaches, J. Mol. Struct. 1116 (2016) 45-55.

[7] P.V. Braun, P. Osenar, V. Tohver, S.B. Kennedy, S.I. Stupp, Nanostructure templating in inorganic solids with organic lyotropic liquid crystals, J. Am. Chem. Soc. 121 (1999) 7302-7309.

[8] M. C. Daniel, D. Astruc, Gold nanoparticles: assembly, supramolecular chemistry, quantum-size-related properties, and applications toward biology, catalysis, and nanotechnology, Chem. Rev. 104 (2004) 293-346.

[9] M.G. Bogaert, Clinical pharmacokinetics of nitrates, Cardiovasc Drugs Ther. 8 (5) (1994) 693-699.

[10] S.A. Brandan (Ed.), Nitrate: Occurrence, Characteristics and Health Considerations, Nova Science Publishers, Inc, 2012, ISBN 978-1-62257-352-3. Edited Collection.

[11] S.A. Brandan, in: Ken Derham (Ed.), A Structural and Vibrational Study of the Chromyl Chlorosulfate, Fluorosulfate, and Nitrate Compounds, vol. 1, Springer Science, Business Media B.V., Van Godewijckstraat 30, 3311 GZ Dordrecht, Netherlands, 2012, ISBN 978-94-007-5762-2.

[12] S.A. Brandan (Ed.), Descriptors, Structural and Spectroscopic Properties of Heterocyclic Derivatives of Importance for the Health and the Enviromental, Nova Science Publishers, Inc, 2015, ISBN 978-1-63482-708-9. Edited Collection.

[13] M.V. Castillo, E. Romano, H.E. Lanús, S.B. Díaz, A. Ben Altabef, S.A. Brandan, Theoretical structural and experimental vibrational study of niobyl nitrate, J. Mol. Struct. 994 (2011) 202-208.

[14] K.E. Torfgård, J. Ahlner, Mechanisms of action of nitrates, Cardiovasc Drugs Ther. 8 (5) (1994) 701 717.

[15] S. Gatfaoui, A. Mezni, T. Roisnel, H. Marouani, Synthesis, characterization, Hirshfeld surface analysis and antioxidant activity of a novel organic-inorganic hybrid material 1-methylpiperazine-1,4-diium bis(nitrate), J. Mol. Struct. 1139 (2017) 52-59.

[16] S. Gatfaoui, N. Issaoui, A. Mezni, F. Bardak, T. Roisnel, A. Atac, H. Marouani, Synthesis, structural and spectroscopic features, and investigation of bioactive nature of a novel organic-inorganic hybrid material 1H-1,2,4-triazole-4-ium trioxonitrate, J. Mol. Struct. 1150 (2017) 242-257.

[17] C.A. Sotriffer, W. Flader, R.H. Winger, B.M. Rode, K.R. Liedl, J.M. Varga Automated docking of ligand to antibodies: methods and applications. Methods 20 (2000) 280–291.

[18] B. Coupez, R.A. Lewis, Docking and scoring theoretically easy, practically impossible, Curr. Med. Chem. 13 (2006) 2995–3003.

[19] O. Noureddine, S. Gatfaoui, S. A. Brandan, H. Marouani, N. Issaoui. Structural, docking and spectroscopic studies of a new piperazine derivative, 1-phenylpiperazine-1,4-diium-bis (hydrogen sulfate), J. Mol. Struct. 1202 (2020) 127351.

[20] H.A Carlson, J.A. Cammon, Accomodating protein flexibility in computational drug design, Mol. Pharmacol. 57 (2000) 213–218.

[21] I. Halperin, H. Wolfson, R. Nussinov, Principles of docking: An overview of search algorithms and a guide to scoring functions, Proteins: Struct. Func. Bioinfo. 47 (2002) 409–443.

[22] R. Abagyan, M. Totrov, High-throughput docking for lead generation, CURR. OPIN. CHEM. BIOL. 5 (2001) 375-382.

[23] Bruker, APEX2, SAINT and SADABS, Bruker AXS Inc., Madison,Wisconsin, USA, 2006.

[24] A. Altomare, M.C. Burla, M. Camalli, G.L. Cascarano, C. Giacovazzo, A. Guagliardi, A. G .G. Moliterni, G. Polidori, R. Spagna, J. Appl. Cryst. 32 (1999) 115.

[25] G. M. Sheldrick, Crystal structure refinement with SHELXL, Acta Cryst. C71 (2015) 3-8.

[26] L. J. Farrugia, WinGX and ORTEP for windows: an update, J. Appl. Cryst. 45 (2012) 849-854.

[27] K. Brandenburg, Diamond Version 2.0 Impact. (GbR, Bonn, 1998).

[28] S. K. Wolff, D. J. Grimwood, J. J. McKinnon, D. Jayatilaka, M. A. Spackamn, Crystal Explorer 3.1, University of Westren Australia, Perth, 2013.

[29] M. J. Frisch, et al., GAUSSIAN 09, Revision A.02, Gaussian, Inc., Wallingford, CT, 2009.

[30] A.D. Becke, Becke's three parameter hybrid method using the LYP correlation functional, J. Chem. Phys. 98 (1993) 5648-5652.

[31] C. Lee, W. Yang, R. G. Parr, Development of the Colle-Salvetti correlation-energy formula into a functional of the electron density, Phys. Rev. B 37 (1988) 785-789.

[32] E. Runge, E.K.U. Gross, Phys. Rev. Lett. 52 (1984) 997-1000.

[33] W. Humphrey, A. Dalke, K. Schulten, VMD—Visual molecular dynamics, J. Mol. Graph. 14 (1996) 33–38 27–8.

[34] E. D. Glendening, J. K. Badenhoop, A. D. Reed, J.E. Carpenter, F. Weinhold, NBO 3.1, Theoretical Chemistry Institute, University of Wisconsin, Madison, WI, Oxford, 1996, ISBN 0198558651, p. 1990.

[35] J.M. Yang, C.C. Chen, GEMDOCK: a generic evolutionary method for molecular docking, Proteins Struct. Funct. Bioinforma. 55 (2004) 288-304.

[35] D.S. Visualizer, Accelrys software inc. Discovery Studio Visualizer 2 (2005).

[37] S. Gatfaoui, H. Marouani, M. Rzaigui, 4-Methylbenzylammonium nitrate, Acta Cryst. E69 (2013) o1453.

[38] S. Gatfaoui, H. Marouani, M. Rzaigui, 1,1,4,7,7-Pentamethyldiethylenetriammonium trinitrate, Acta Cryst. E70 (2014) o198.

[39] S. Gatfaoui, H. Dhaouadi, T. Roisnel, M. Rzaigui, H. Marouani, m-Xylylenediaminium dinitrate, Acta Cryst. E70 (2014) o398–o399.

[40] S. Gatfaoui, H. Marouani, T. Roisnel, H. Dhaouadi, Dopaminium nitrate, Acta Cryst. E70 (2014) o571–o572.

[41] S. Gatfaoui, Thierry Roisnel, H. Dhaouadi, H. Marouani, trans-2,5-Dimethylpiperazine-1,4-diium dinitrate, Acta Cryst. E70 (2014) o725.

[42] C. Ben M'leh, S. A. Brandan, N. Issaoui, T. Roisnel, H. Marouani, Synthesis, molecular structure, vibrational and theoretical studies of a new non-centrosymmetric organic sulphate with promising NLO properties, J. Mol. Struct. 1171 (2018) 771-785.

[43] I. D. Brown, Acta Cryst, (1976) A32, 24.

[44] R. H. Blessing, Acta Cryst, (1986) B42, 613.

[45] S. Gatfaoui, N. Issaoui, T. Roisnel, H. Marouani, A proton transfer compound template phenylethylamine: Synthesis, a collective experimental and theoretical investigations, J. Mol. Struct. 1191 (2019) 183-196.

[46] S. Gatfaoui, N. Issaoui, S. A. Brandan, T. Roisnel, H. Marouani, Synthesis and characterization of p-xylylenediaminium bis(nitrate).Effects of the coordination modes of nitrate groups on their structural and vibrational properties, J. Mol. Struct. 1151 (2018) 152-168.

[47] R.F.W. Bader, Atoms in Molecules: A Quantum Theory, Oxford University Press, Oxford, (1990).

[48] E. Espinosa, I. Alkorta, I. Rozas, J. Elguero, R. Molins, J. Chem. Phys. Lett., 336

[49] I. Majerz, A. Koll, Acta Crystallogr. B60 (2004) 406.

[50] P. L. A. Popelier, R. F. W. Bader, J. Phys. Chem. 98 (1994) 4473.

[51] U. Koch, P. L. A. Popelier, J. Phys. Chem. 99 (1995) 9747.

[52] E. Espinosa, I. Alkorta, I. Rozas, J. Elguero, R. Molins, J. Chem. Phys. Lett., 336 (2001) 457.

[53] I. Rozas, I. Alkorta, J. Elguero, Behavior of ylides containing N, O, and C atoms as hydrogen bond acceptors, J. Am. Chem. Soc. 122 (2000) 11154-11161.

[54] E.R. Johnson, S. Keinan, P. Mori-Sánchez, J. Contreras-García, A.J. Cohen, W. Yang, J. Am. Chem. Soc. 132 (2010) 6498–6506.

[55] R.S. Mulliken, J. Chem. Phys. 2 (1934) 782–793.

[56] R.G. Pearson, Chemical Hardness, John Wiley-VCH, Weinheim, 1997.

[57] R.G. Parr, L. von Szentpaly, S. Liu, J. Am. Chem. Soc. 121 (1999) 1922–1924.

[58] A.E. Reed, F. Weinhold, J. Chem. Phys. 83 (1985) 1736–1740.

[59] B. Kosar, C. Albayrak, Spectrochim. Acta A78 (2011) 160–167.

[60] S. Gunasekaran, S. Kumaresan, R. Arunbalaji, G. Anand, S. Srinivasan, J. Chem. Sci. 120 (2008) 315.

[61] R.S. Mulliken, J. Chem. Phys. 23 (1955) 1833.

[62] http://dx.doi.org/10.2210/pdb6W63/pdb.

[63] http://dx.doi.org/10.2210/pdb6W4B/pdb.

[64] E. Kose, A. Atac, F. Bardak, J. Mol. Struct. 10 (2018) 2-99.

[65] F. Weinhold, C. Landis, Valency and Bonding: A Natural Bond Orbital Donor-Acceptor Perspective, Cambridge University Press, Cambridge, 2005.

Figure Captions

Fig. 1. ORTEP drawing of 1EPBN with the atom-labeling scheme. Displacement ellipsoids are drawn at the 30% probability level. H atoms are represented as small spheres of arbitrary radii. (i) : x, -y+1/2, z.

Fig. 2. Projection along the $\vec{a}$ and $\vec{b}$ axis of atomic arrangement of 1EPBN.

Fig. 3. Hydrogen bond motifs in 1EPBN compound.

Fig. 4. The optimized structure of 1EPBN molecule calculated at B3LYP/6-311++G(d,p) level of theory.

Fig. 5. d_{norm} cartography ((a) and (c)) and fingerprints plots ((b) and (d)) of H…O/O…H and H…H contacts existing in 1EPBN molecule.

Fig. 6. Percentage of all contacts present in the 1EPBN material.

Fig. 7. AIM graphs of the studied compound mapped throughout Multiwfn program at B3LYP/6-311++G(d,p) level of theory.

Fig. 8. Reduced density gradient (a) and isosurface density (b) plot along with the color filled scale bar defining interaction limits for the 1EPBN compound.

Fig. 9. Frontier molecular orbital (a) and energitical parameters of 1EPBN crystal.

Fig. 10. MEP and Mullikan charges of 1EPBN compound.

Fig. 11. The corresponding docking position for 6W63 and 6W4B of 1EPBN represented via discovery studio.

Fig. 12. Intermolecular interactions of the title compound with two coronavirus proteins.

Fig. 13. Visual interaction representation of residues and 1EPBN in both complexes.

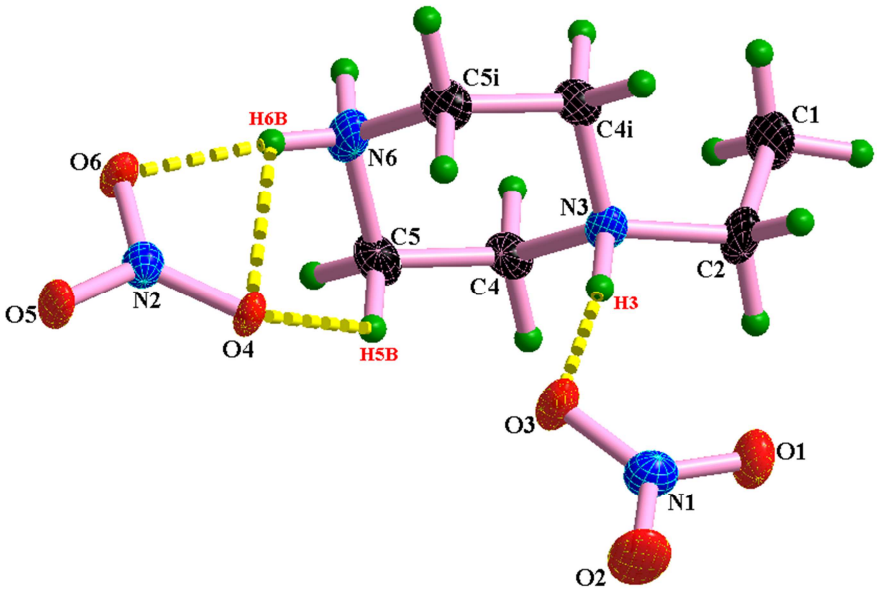
C5i
C4i
C1
H6B
N6
O6
N3
C5
C2
C4
O5
N2
H3
O4
H5B
O3
O1
N1
O2

Fig.1

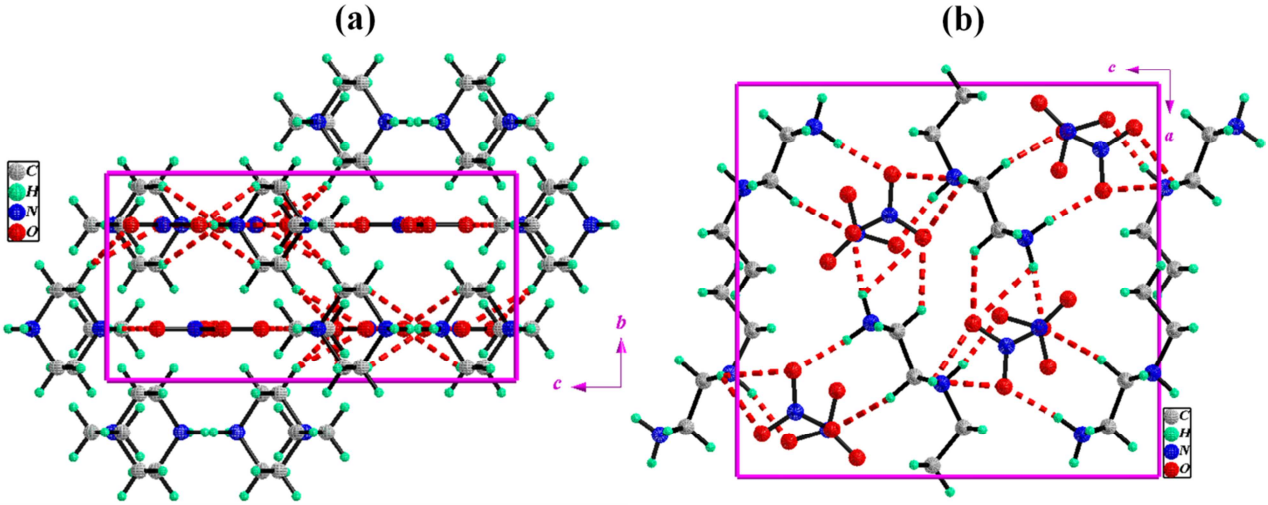
(a)
(b)
C
H
N
O
b
c
c
a

Fig.2

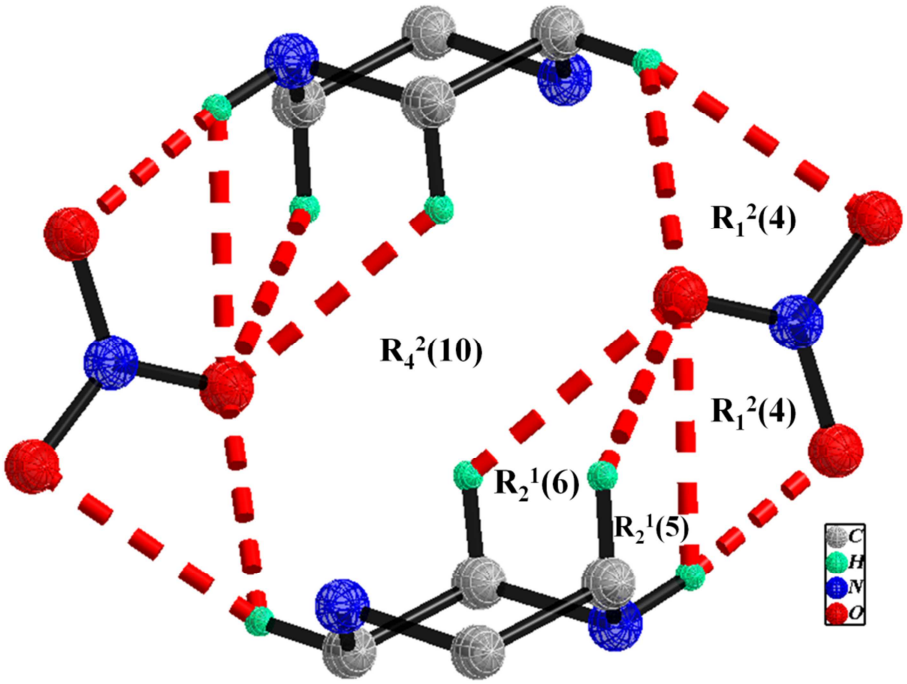
R1²(4)
R4²(10)
R1²(4)
R2¹(6)
R2¹(5)
C
H
N
O

Fig.3

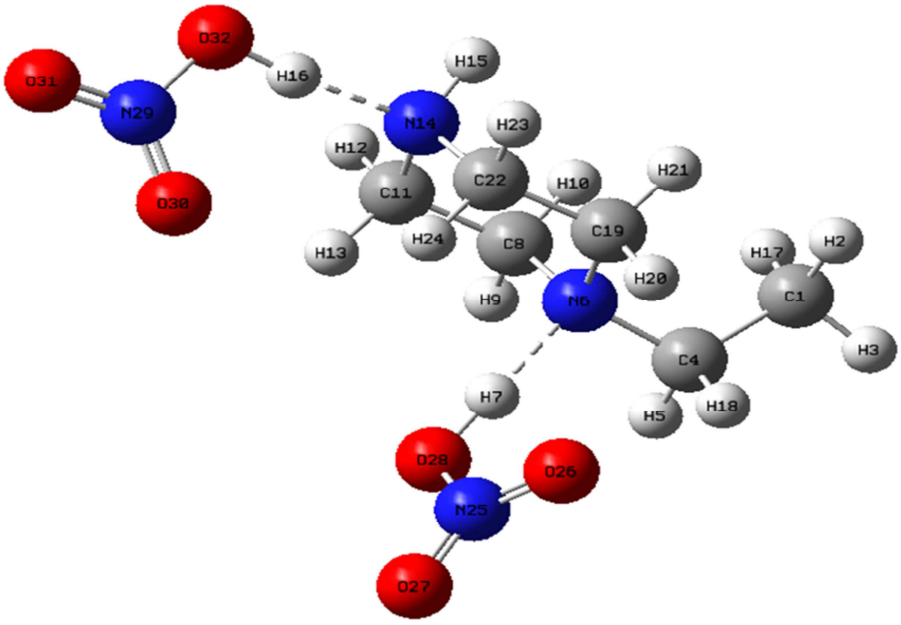
O32
O31
H16
H15
N29
N14
H23
H12
C22
H10
H21
C11
O30
H24
C19
H13
C8
H17
H2
H20
H9
N6
C1
H3
C4
H7
H5
H18
O28
O26
N25
O27

Fig.4

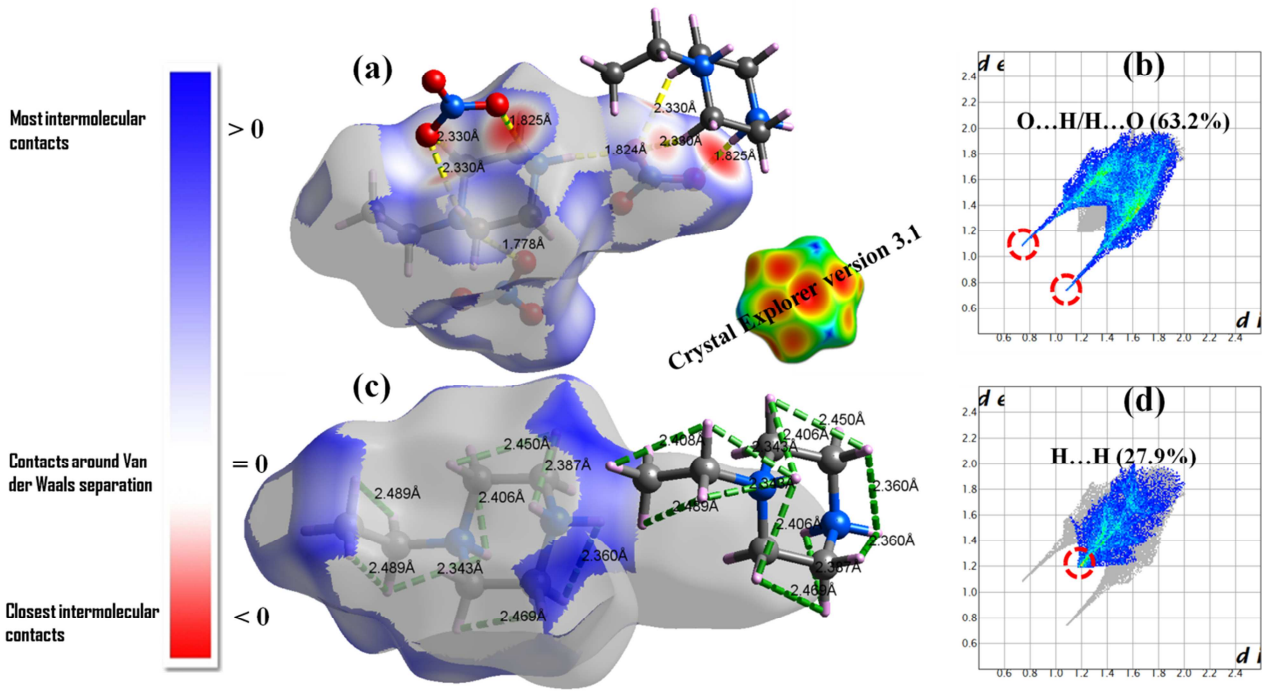
Most intermolecular contacts
> 0
Contacts around Van der Waals separation
= 0
Closest intermolecular contacts
< 0
(a)
(b)
O…H/H…O (63.2%)
(c)
(d)
H…H (27.9%)
Crystal Explorer version 3.1

Fig.5

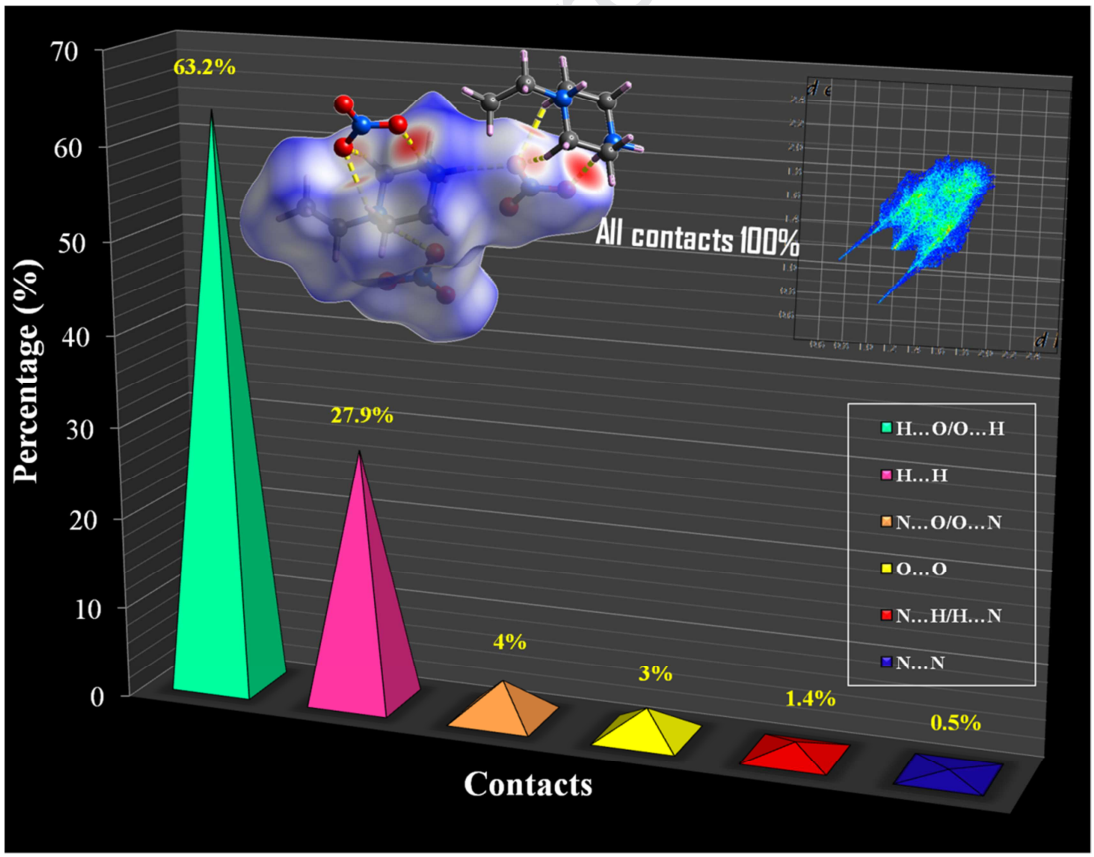
Percentage (%)
70
60
50
40
30
20
10
0
63.2%
27.9%
4%
3%
1.4%
0.5%
All contacts 100%
H…O/O…H
H…H
N…O/O…N
O…O
N…H/H…N
N…N
Contacts

Fig.6

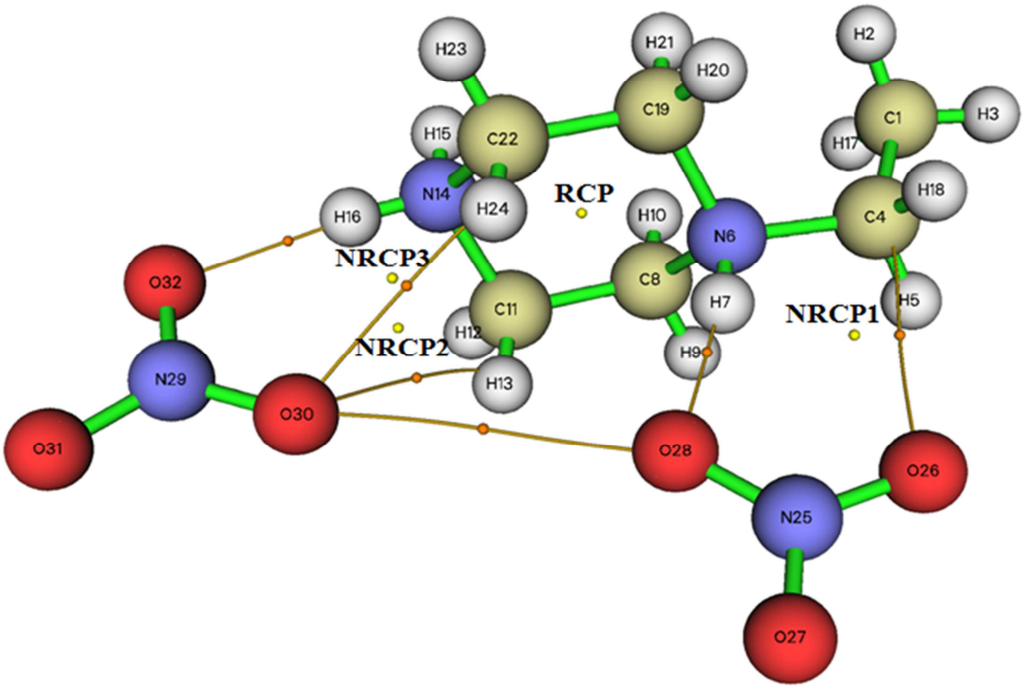
H23
H21
H20
H2
C19
C1
H3
H15
C22
H17
N14
H24
RCP
H18
H16
H10
N6
C4
NRCP3
O32
C8
H7
C11
NRCP1
H5
H12
NRCP2
H9
N29
H13
O30
O31
O28
O26
N25
O27

Fig.7

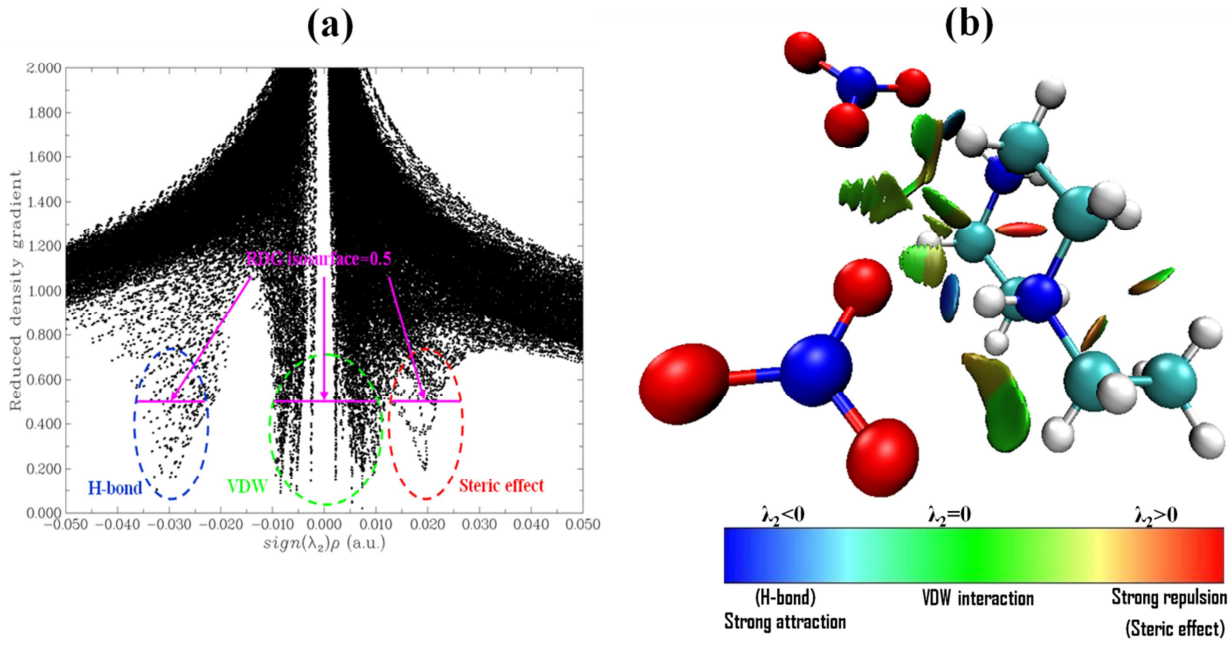
(a)
(b)
Reduced density gradient
RDG isosurface=0.5
H-bond
VDW
Steric effect
sign(λ2)ρ (a.u.)
λ2<0
λ2=0
λ2>0
(H-bond)
Strong attraction
VDW interaction
Strong repulsion
(Steric effect)

Fig.8

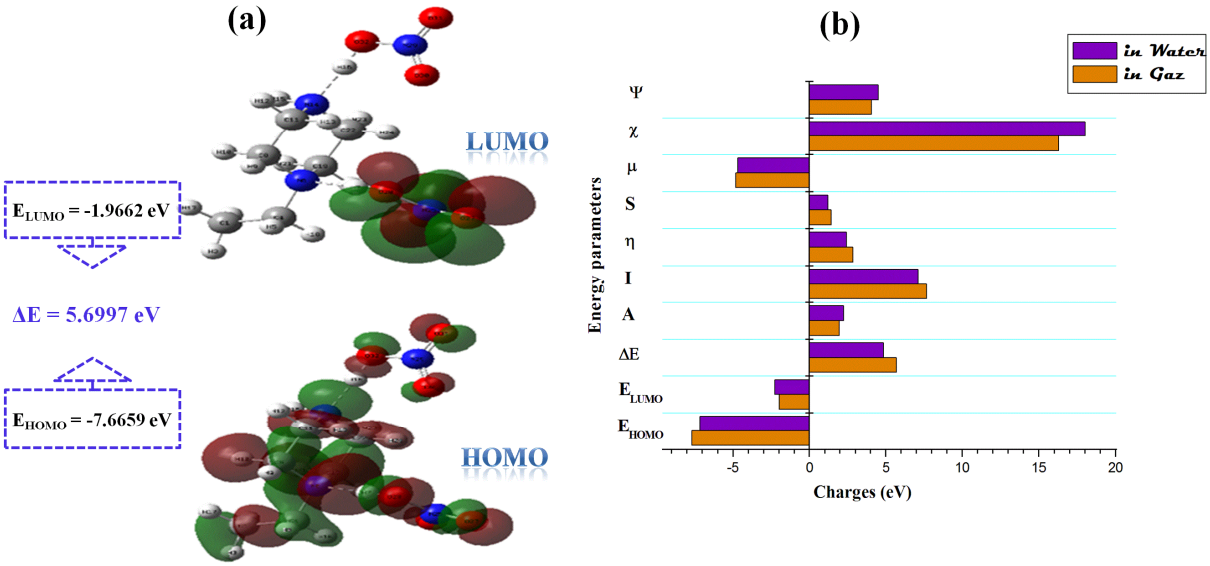

Fig.9

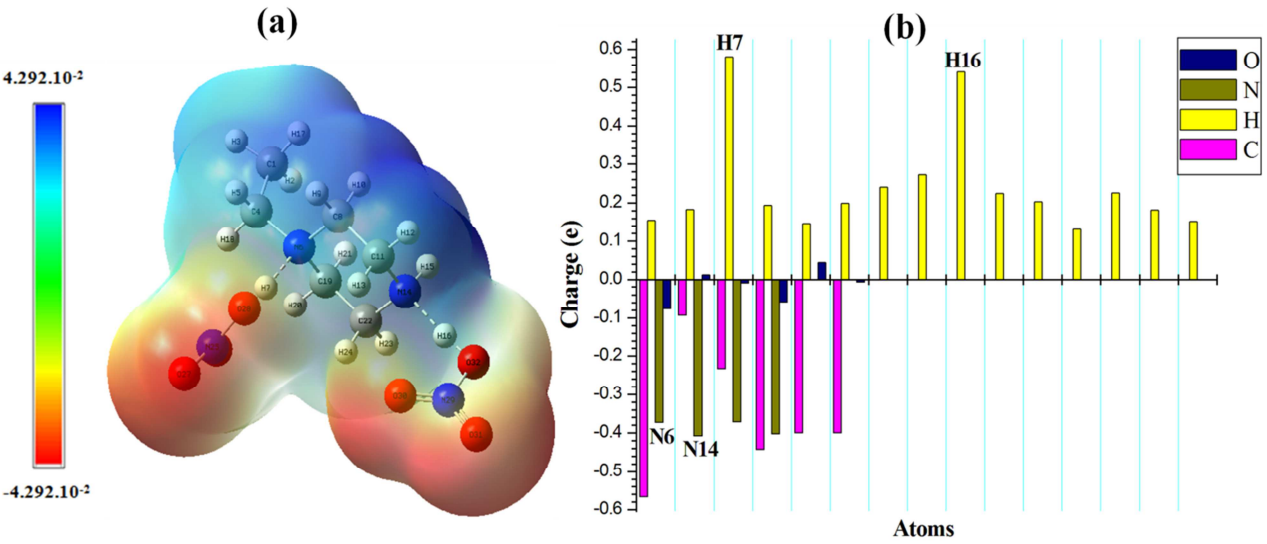

Fig.10

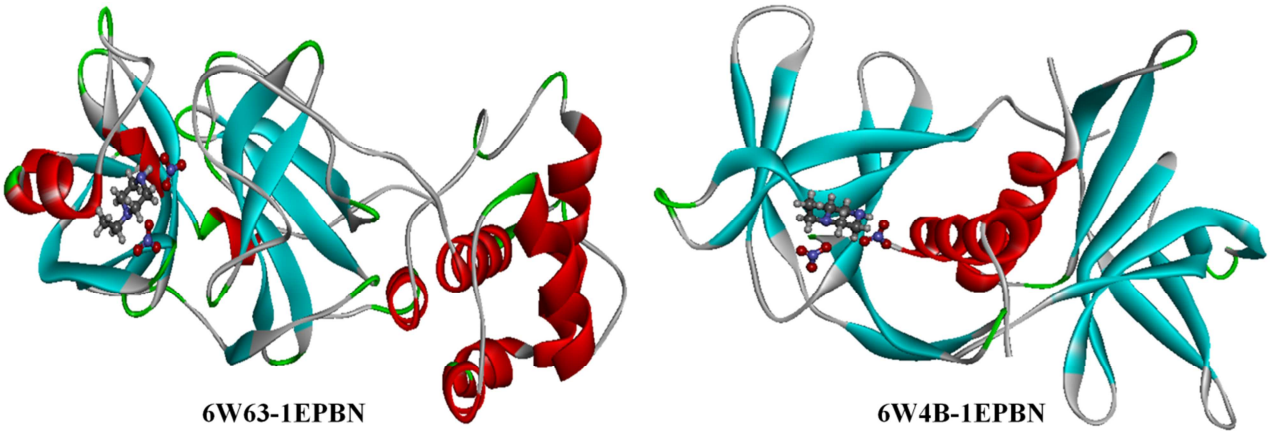

Fig.11

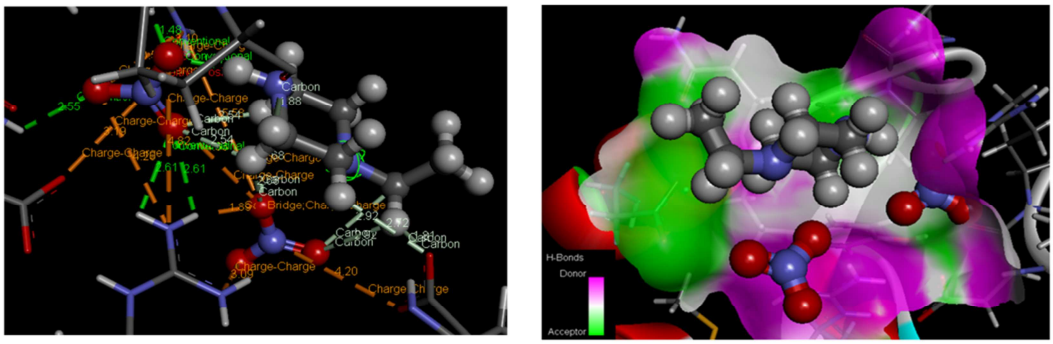

6W63-1EPBN

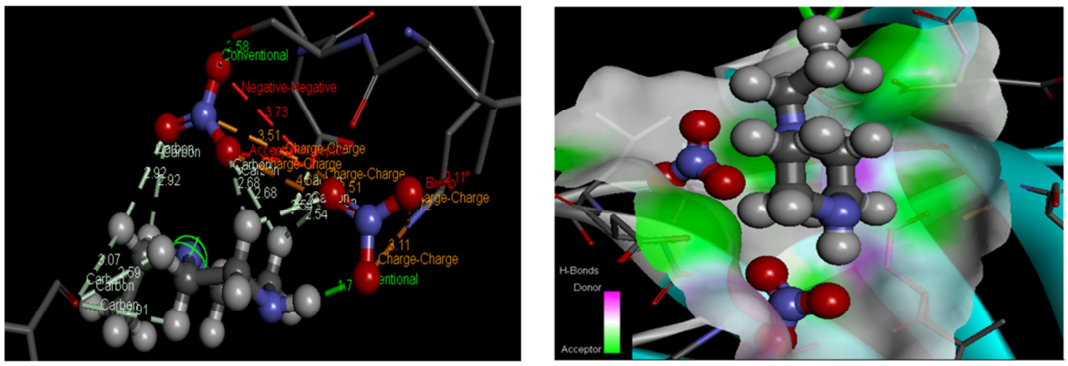

6W4B-1EPBN

Fig.12

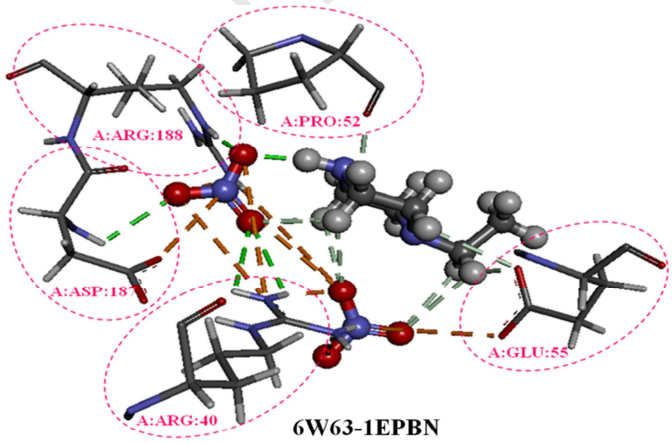

6W63-1EPBN

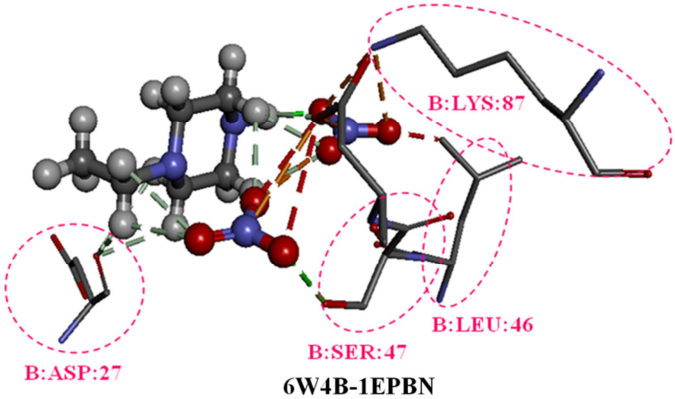

6W4B-1EPBN

Fig.13

Table captions

Table 1 Crystal data and experimental parameters used for the intensity data collection strategy and final results of the structure determination.

Table 2 Theoretical and experimental bond lengths and bond angles of the title compound.

Table 3 Hydrogen-bond geometry (Å,°) of 1EPBN.

Table 4 Topological parameters of the title compound calculated at DFT/B3LYP/6-311++G(d,p).

Table 5 Calculated energy value for the studied compound by using TD-B3LYP/6-311++G(d,p) method.

Table 6 Mulliken charge distribution of the title compound calculated by B3LYP method using 6-311++G(d,p) basis set.

Table 7 Docking studies of the title compound with two coronavirus proteins (COVID-19 and SARS-CoV2).

Table 8 Natural Bond Orbitals calculations of 1EPBN.

Table 1

CCDC	1996865
Empirical formula	$C_6 H_{16}N_2(NO_3)_2$
Temperature	150 K
Formula weight (g mol^{-1})	240.23
Crystal system	Orthorhombic
Space group	Pnma
a, b, c (Å)	12.158(2), 6.5939(9), 13.058(2)
Z	4
V($Å^3$)	1046.8(3)
F(000)	512
Radiation type	Mo Kα
μ(mm^{-1})	0.135
Crystal size (mm)	0.54 x 0.30 x 0.13
Index ranges	$-15 \leq h \leq 15$, $-7 \leq k \leq 8$, $-16 \leq l \leq 16$
Reflections collected	6291
Independent reflections	1297
Reflections with $I > 2\sigma(I)$	1185
R_{int}	0.0308
Diffractometer	D8 VENTURE Bruker AXS
Absorption correction	Multi-scan
T_{min}, T_{max}	0.903, 0.983
Refined parameters	102
$R_1[F^2 > 2\sigma(F^2)]$	0.035
$wR_2(F^2)$	0.096
Goodness of fit	1.06
$\Delta\rho_{max}$, $\Delta\rho_{min}$ ($eÅ^{-3}$)	0.23, -0.41

$R_1 = \sum | |F_o| - |F_c| | / \sum |F_o|$; $wR_2 = \{\sum [w(F_o^2 - F_c^2)^2] / \sum [w(F_o^2)^2]\}^{1/2}$

Table 2

Parameters	B3LYP/6-311++G(d, p)	Exp	Parameters	B3LYP/6-311++G(d,p)	Exp	Parameters	B3LYP/6-311++G(d,p)	Exp
Bond Length (Å)								
C1-H2	1.0923	0.969(13)	C8-H9	1.0938	0.9900	C19-H21	1.1008	0.9900
C1-H3	1.0929	0.98(2)	C8-H10	1.1006	0.9900	C19-C22	1.5286	0.9900
C1-C4	1.5324	1.522(2)	C8-C11	1.53	1.5160(13)	C22-H23	1.0923	0.9900
C1-H17	1.0925	0.969(13)	C11-H12	1.0924	0.9900	C22-H24	1.0923	0.9900
C4-H5	1.0944	0.9900	C11-H13	1.0928	0.9900	N25-O26	1.2237	1.2473(17)
C4-N6	1.4853	1.5074(17)	C11-N14	1.478	1.4961(12)	N25-O27	1.2024	1.2437(16)
C4-H18	1.0931	0.9900	N14- H15	1.0195	0.91(2)	N25-O28	1.3707	1.2613(16)
N6-H7	1.6216	0.902(19)	N14-H16	1.6221	0.915(19)	N29-O30	1.2219	1.2407(15)
N6-C8	1.4764	1.4997(11)	N14-C22	1.4788	1.4961(12)	N29-O31	1.2035	1.2665(16)
N6-C19	1.4779	1.4997(11)	H16-O32	1.038		N29-O32	1.3722	1.2592(15)
H7-O28	1.043		C19-H20	1.0918	0.9900	**RMSD**		
Bond Angles (°)								
H2-C1-H3	107.2622	109.8(10)	N6-C8-C11	110.6618	110.10(8)	H20-C19-C22	109.7234	109.6
H2-C1-C4	112.3405	111.1(8)	H9-C8-H10	107.5874	108.2	H21-C19-C22	109.3354	109.6
H2-C1-H17	108.396	109.8(10)	H9-C8-C11	109.8217	109.6	N14-C22-C19	112.5668	110.28(8)
H3-C1-C4	108.8147	106.9(12)	H10-C8-C11	109.2953	109.6	N14-C22-H23	108.7581	109.6
H3-C1-H17	107.2805	109.8(10)	C8-C11-H12	109.9176	109.6	N14-C22-H24	107.3186	109.6
C4-C1-H17	112.4952	111.1(8)	C8-C11-H13	110.5316	109.6	C19-C22-H23	109.8831	109.6
C1-C4-H5	109.543	108.8	C8-C11-N14	112.3767	110.28(8)	C19-C22-H24	110.5506	109.6
C1-C4-N6	117.2938	113.77(11)	H12-C11-H13	107.7164	108.1	H23-C22-H24	107.603	108.1
C1-C4-H18	109.8264	108.8	H12-C11-N14	108.7967	109.6	O26-N25-O27	127.6402	121.24(13)
H5-C4-N6	106.5543	108.8	H13-C11-N14	107.3544	109.6	O26-N25-O28	116.8497	119.26(12)
H5-C4-H18	106.7927	107.7	C11-N14-H15	109.0022	108.3(6)	O27-N25-O28	115.51	119.50(12)
N6-C4-H18	106.2981	108.8	C11-N14-H16	110.9644	109.9(6)	H7-O28-N25	107.3769	
C4-N6-H7	100.7292	105.7(12)	C11-N14-C22	110.6102	111.20(10)	O30-N29-O31	127.7517	120.19(11)
C4-N6-C8	113.2834	112.65(7)	H15-N14-H16	106.4328	112.65(7)	O30-N29-O32	116.8736	120.19(11)

C4-N6-C19	113.0503	112.65(7)	H15-N14-C22	109.0145	108.3(6)	O31-N29-O32	115.3746	119.58(11)
H7-N6-C8	107.9381	107.9(6)	H16-N14-C22	110.6963	109.9(6)	H16-O32-N29	107.0695	
H7-N6-C19	110.1296	107.9(6)	N6-C19-H20	108.092	109.6			
C8-N6-C19	111.0995	109.72(10)	N6-C19-H21	110.7531	109.6			
N6-C8-H9	108.4419	109.6	N6-C19-C22	110.6844	110.10(8)			
N6-C8-H10	110.9736	109.6	H20-C19-H21	108.205	108.2			

Table 3

D—H···*A*	*D*—H (Å)	H···*A* (Å)	*D*···*A* (Å)	*D*—H···*A*(°)
N3—H3···O3	0.902(19)	1.884(19)	2.7757(16)	169.9(17)
N6—H6A···O5^{ii}	0.915(19)	1.92(2)	2.8304(16)	174.4(17)
N6—H6B···O6	0.91(2)	1.92(2)	2.8269(16)	172.5(17)
N6—H6B···O4	0.91(2)	2.574(19)	3.0982(16)	117.1(14)
C4—H4A···O4^{iii}	0.99	2.52	3.1985(12)	125.3
C4—H4B···O5^{iii}	0.99	2.56	3.4726(13)	153.5
C4—H4B···O6^{ii}	0.99	2.41	3.2760(13)	146.2
C4—H5B···O4	0.99	2.60	3.2535(14)	123.9

Symmetry codes: (ii) $x-1/2, y, -z+1/2$; (iii) $-x+1, y+1/2, -z+1$.

Table 4

Interactions	**ρ(r) (u.a)**	**Δρ(r) (u.a)**	**λ_1**	**λ_2**	**λ_3**	**H(r) (u.a)**	**G(r) (u.a)**	**V(r) (u.a)**	**E_{int} (kJ.mol^{-1})**
O_{26}-H_5	0.0065	0.0249	-0.0038	0.0307	-0.0018	0.0010	0.0051	-0.0040	-0.0020
O_{28}-H_7	0.0327	0.1085	-0.0487	0.2032	-0.0459	0.0006	0.0265	-0.0259	-0.0129
O_{30}-O_{28}	0.0025	0.0118	0.0147	-0.0014	-0.0015	0.0005	0.0023	-0.0017	-0.0008
O_{30}-H_{13}	0.0084	0.0279	0.0413	-0.0056	-0.0076	0.0010	0.0059	-0.0049	-0.0024
O_{30}-H_{24}	0.0084	0.0279	0.0413	-0.0056	-0.0076	0.0010	0.0059	-0.0049	-0.0024
O_{32}-H_{16}	0.0297	0.0952	0.1791	-0.0432	-0.0406	0.0008	0.0229	-0.0220	-0.0110
RCP1	0.0193	0.1209	0.0606	-0.0161	0.0764	0.0057	0.0245	-0.0188	-
NRCP1	0.0060	0.0249	0.0047	0.0234	-0.0032	0.0011	0.0051	-0.0040	-
NRCP2	0.0073	0.0301	0.0065	0.0284	-0.0048	0.0012	0.0062	-0.0050	-
NRCP3	0.0073	0.0301	0.0065	0.0284	-0.0048	0.0012	0.0062	-0.0050	-

Table 5

	Gas	Water
E_{HOMO}(eV)	-7.6659	-7.1193
E_{LUMO}(eV)	-1.9662	-2.2514
$\Delta E_{HOMO-LUMO}$ (eV)	-5.6997	-4.8675
Electronic affinity A (eV)	1.9662	2.2514
Ionization potential I (eV)	7.6659	7.1193
Chemical hardness η (eV)	2.8498	2.4339
Softness S (eV)	1.4249	1.2169
Chemical potentiel μ (eV)	-4.8160	-4.6853
Electronegativity χ (eV)	16.2774	18.0392
Electrophilicity ψ (eV)	4.0693	4.5108

Table 6

Atoms	B3LYP/6-311++G(d,p)	Atoms	B3LYP/6-311++G(d,p)
C1	-0.565566	H17	0.151350
H2	0.154232	H18	0.180872
H3	0.163444	C19	-0.399428
C4	-0.093885	H20	0.225108
H5	0.182434	H21	0.131496
N6	-0.373457	C22	-0.399250
H7	0.580630	H23	0.201516
C8	-0.233306	H24	0.223597
H9	0.192224	N25	-0.402304
H10	0.145682	O26	-0.008038
C11	-0.442465	O27	0.044233
H12	0.197944	O28	-0.058477
H13	0.240285	N29	-0.371714
N14	-0.407403	O30	-0.010098
H15	0.272180	O31	0.012095
H16	0.541590	O32	-0.075521

Table 7

Protein Name	Code	Total Energy E_{int} (kcal/mol)	VDW	H-bond	Elec	Binding Residues	Atoms	Distance	Interaction category
COVID-19	6W63	-84.32	-34.54	-51.59	1.81	A:ARG:40	O28	1.89	
							O27	3.08	Electrostatic
							O31	4.26	
							O32	4.82	
							O30	4.6	H-bond
						A:ARG:188	O28	5.57	
							O31	3.5	Electrostatic
							O32	3.01	
							O32	1.47	H-bond
						Z:PRE:999	N25	4.20	
							N29	3.2	Electrostatic
							O28	4.62	
							O32	1.78	H-bond
							O26	2.92	
							H20	1.81	Carbon H-bond
							O28	2.68	
							O30	2.53	
						A:ASP:187	O31	2.54	H-bond
SARS-CoV2	6W4B	-68.15	-29.45	-37.85	-0.86	B:LYS:87	O31	2.71	Electrostatic
							O32	3.10	
						Z:PRE:999	N25	3.51	Electrostatic
							O28	4.62	
							O32	1.76	
							O26	2.92	
							N25	2.22	Carbon H-bond
							O28	2.68	
							O30	2.53	
						B:SER:47	O27	2.58	H-bond

Table 8

Donor(i)	Acceptor(j)	$E^{(2)}$	E(j)-E(i)	F(i,j)	Donor(i)	Acceptor(j)	$E^{(2)}$	E(j)-E(i)	F(i,j)
Within unit1									
σ (C1-H2)	σ (C4-H5)	2.39	0.91	0.042	σ (C11-H13)	σ (N14-H15)	3.12	0.88	0.047
σ (C1-H3)	σ (C4-N6)	4.73	0.82	0.056	σ (C11-N14)	σ (C8-H9)	1.02	1.13	0.030
σ (C1-H17)	σ (C4-H18)	2.33	0.92	0.041	σ (C11-N14)	σ (C22-H23)	1.21	1.12	0.033
σ (C4-H5)	σ (C1-H2)	2.72	0.91	0.045	σ (N14-H15)	σ (C11-H13)	1.91	1.03	0.040
σ (C4-H5)	σ (N6-C19)	3.72	0.83	0.050	σ (N14-H15)	σ (C22-H24)	1.91	1.03	0.040
σ (C4-N6)	σ (C1-H3)	0.64	1.12	0.024	σ (N14-C22)	σ (C11-H12)	1.23	1.12	0.033
σ (C4-N6)	σ (N6-C8)	0.68	1.03	0.024	σ (N14-C22)	σ (C19-H20)	0.97	1.14	0.030
σ (C4-N6)	σ (N6-C19)	0.70	1.03	0.024	σ (C19-H20)	σ (N6-C8)	3.63	0.83	0.049
σ C4-N6	σ (C8-C11)	1.39	1.08	0.035	σ (C19-H20)	σ (N14-C22)	3.79	0.83	0.050
σ (C4-N6)	σ (C19-C22)	1.36	1.08	0.034	σ (C19-H21)	σ (C22-H24)	2.46	0.92	0.043
σ (C4-H18)	σ (C1-H17)	2.73	0.91	0.045	σ (C19-C22)	σ (C4-N6)	2.67	0.95	0.045
σ (C4-H18)	σ (N6-C8)	3.83	0.82	0.050	σ (C19-C22)	σ (C19-H20)	0.60	1.05	0.022
σ (N6-C8)	σ (C4-N6)	0.60	1.03	0.022	σ (C22-H23)	σ (N6-C19)	3.41	0.83	0.048
σ (N6-C8)	σ (C4-H18)	0.79	1.13	0.027	σ (C22-H23)	σ (C11-N14)	3.38	0.83	0.047
σ (N6-C8)	σ (N6-C19)	0.63	1.03	0.023	σ (C22-H24)	σ (N14-H15)	3.12	0.88	0.047
σ (N6-C8)	σ (C11-H12)	0.97	1.11	0.029	σ (C22-H24)	σ (C19-H21)	2.69	0.89	0.044
σ (N6-C8)	σ (C19-H20)	1.06	1.13	0.031	LP(1)N6	σ (C1-C4)	5.74	0.69	0.059
σ N6-C19)	σ (C4-H5)	0.83	1.12	0.027	LP(1)N6	σ (C4-H5)	1.41	0.72	0.030
σ (N6-C19)	σ (C4-N6)	0.61	1.03	0.023	LP(1)N6	σ (C4-H18)	1.28	0.73	0.029
σ (N6-C19)	σ (N6-C8)	0.64	1.03	0.023	LP(1)N6	σ (C8-H9)	1.11	0.72	0.026
σ (N6-C19)	σ ((C8-H9)	1.14	1.11	0.032	LP(1)N6	σ (C8-H10)	6.41	0.70	0.062
σ (N6-C19)	σ (C22-H23)	0.97	1.11	0.029	LP(1)N6	σ (C8-C11)	0.81	0.69	0.022
σ (C8-H9)	σ (N6-C19)	3.55	0.84	0.049	LP(1)N6	σ (C19-H20)	1.08	0.74	0.026
σ (C8-H9)	σ (C11-N14)	3.70	0.84	0.050	LP(1)N6	σ (C19-H21)	6.30	0.70	0.062
σ (C8-H10)	σ (C11-H13)	2.44	0.92	0.042	LP(1)N6	σ (C19-C22)	0.80	0.69	0.022
σ (C8-C11)	σ (C4-N6)	2.69	0.95	0.045	LP(1)N14	σ (C8-C11)	5.25	0.71	0.056
σ (C8-C11)	σ (C8-H9)	0.56	1.03	0.022	LP(1)N14	σ (C11-H12)	0.76	0.74	0.022
σ (C11-H12)	σ (N6-C8)	3.36	0.83	0.047	LP(1)N14	σ (C11-H13)	1.56	0.74	0.032
σ (C11-H12)	σ (N14-C22)	3.36	0.84	0.047	LP(1)N14	σ (C19-C22)	5.17	0.72	0.056
σ (C11-H13)	σ (C8-H10)	2.67	0.89	0.043	LP(1)N14	σ (C22-H23)	0.75	0.74	0.022
σ (C11-H13)	σ (N14-H15)	3.12	0.88	0.047					
From unit1 to unit 2									

σ (C4-N6)	σ (H7-O28	0.99	1.03	0.029	σ (C11-H13)	σ (H7-O28)	0.05	0.83	0.006
σ (N6-C8)	σ (H7-O28)	0.67	1.04	0.024	σ (C19-H21)	σ (H7-O28)	0.12	0.84	0.009
σ (N6-C19)	σ (H7-O28)	0.61	1.04	0.023	LP(1)N6	σ (H7-O28)	40.01	0.64	0.146
σ (C8-H10)	σ (H7-O28)	0.11	0.84	0.009					
From unit1 to unit 3									
σ (C8-C11)	σ (H16-O32)	0.09	0.97	0.008	σ (N14-C22)	σ H16-O32)	0.78	1.07	0.026
σ (C11-N14)	σ (H16-O32)	0.77	1.07	0.026	σ (C19-C22)	σ (H16-O32)	0.09	0.97	0.008
σ (N14-H15)	σ (H16-O32)	0.85	0.97	0.026	LP(1)N14	σ (H16-O32)	44.48	0.69	0.158
From unit 2 to unit1									
σ (H7-O28)	σ (N6-C8)	0.09	1.08	0.009	LP(3)O26	σ (C4-H18)	0.09	0.69	0.008
σ (H7-O28)	σ (N6-C19	0.13	1.08	0.010	LP(2)O28	σ (C1-C4)	0.10	0.70	0.008
LP(1)O26	σ (C4-H18)	0.07	1.22	0.008	σ (H7-O28)	σ (C1-C4)	0.44	0.05	0.016
LP(1)O26	σ (C19-H20)	0.08	1.23	0.009	σ (H7-O28)	σ (C11-H12)	0.05	0.07	0.007
LP(1)O26	σ (C19-H21)	0.07	1.19	0.008	σ (H7-O28)	σ (C11-H13)	0.11	0.08	0.010
LP(2)O26	σ (C4-H18)	0.08	0.71	0.007	σ (H7-O28)	σ (C19-H21)	0.06	0.06	0.006
LP(2)O26	σ (C19-H20)	0.11	0.71	0.008	σ (H7-O28)	σ (C22-H23)	0.06	0.07	0.008
LP(2)O26	σ (C19-H21)	0.16	0.67	0.009	σ (H7-O28)	σ (C22-H24)	0.12	0.08	0.010
Within unit 2									
σ (H7-O28)	π (N25-O27)	4.50	1.23	0.067	LP(1)O27	σ (N25-O26)	4.67	1.22	0.068
σ (H7-O28)	σ (N25-O28)	0.64	0.93	0.023	LP(1)O27	σ (N25-O28)	1.93	0.97	0.040
σ (N25-O27)	σ (N25-O27)	9.67	0.34	0.061	LP(2)O27	σ (N25-O26)	17.36	0.71	0.101
π (N25-O27)	σ (H7-O28)	1.23	1.45	0.039	LP(2)O27	σ (N25-O28)	29.35	0.46	0.104
LP(1)O26	σ (H7-O28)	0.67	1.13	0.025	LP(1)O28	σ (N25-O26)	5.75	1.08	0.071
LP(1)O26	π (N25-O27)	4.42	1.28	0.068	LP(2)O28	σ (N25-O27)	39.67	0.20	0.091
LP(1)O26	σ (N25-O28)	1.68	0.98	0.038	σ (H7-O28)	σ (N25-O26)	1.00	0.10	0.030
LP(2)O26	σ (H7-O28)	0.86	0.62	0.021	σ (N25-O27)	π (N25-O27)	1.13	0.60	0.040
LP(2)O26	π (N25-O27)	15.30	0.76	0.098	σ (N25-O28)	σ (H7-O28)	1.03	0.15	0.030
LP(2)O26	σ (N25-O28)	25.49	0.47	0.098	σ (N25-O28)	σ (N25-O26)	0.53	0.25	0.030
LP(3)O26	σ (N25-O27)	144.83	0.15	0.138					
From unit 3 to unit 1									
σ (H16-O32)	σ (C11-N14)	0.08	1.07	0.008	σ (H16-O32)	σ (C11-N14)	0.08	1.07	0.008
σ (H16-O32)	σ (N14-C22)	0.07	1.08	0.008	σ (H16-O32)	σ (N14-C22)	0.07	1.08	0.008
LP(1)O30	σ (C11-H13)	0.11	1.21	0.010	LP(1)O30	σ (C11-H13)	0.11	1.21	0.010
LP(1)O30	σ (C22-H24)	0.14	1.21	0.012	LP(1)O30	σ (C22-H24)	0.14	1.21	0.012

LP(2)O30	σ (C11-H13)	0.07	0.69	0.006	LP(2)O30	σ (C11-H13)	0.07	0.69	0.006
Within unit 3									
σ (H16-O32)	π (N29-O31	4.55	1.23	0.067	LP(3)O30	σ (N29-O31)	152.02	0.15	0.139
σ (H16-O32)	σ (N29-O32)	0.71	0.93	0.024	LP(1)O31	σ (N29-O30)	4.68	1.23	0.068
σ (N29-O31)	σ N29-O31	9.90	0.33	0.062	LP(1)O31	σ (N29-O32)	1.88	0.97	0.040
π (N29-O31)	σ H16-O32	1.07	1.47	0.036	LP(2)O31	σ (N29-O30)	17.13	0.72	0.101
σ (N29-O32)	σ N29-O32	0.52	1.09	0.022	LP(2)O31	σ (N29-O32)	29.27	0.46	0.104
LP(1)O30	σ H16-O32	0.52	1.15	0.022	LP(1)O32	σ (N29-O30)	5.62	1.09	0.070
LP(1)O30	π (N29-O31)	4.56	1.28	0.069	LP(2)O32	σ (N29-O31)	40.13	0.20	0.091
LP(1)O30	σ N29-O32	1.63	0.98	0.037	σ (H16-O32)	σ (N29-O30)	1.19	0.09	0.032
LP(2)O30	σ H16-O32	0.82	0.63	0.020	σ (N29-O32)	σ (H16-O32)	0.87	0.17	0.029
LP(2)O30	π (N29-O31)	15.39	0.76	0.099	σ (N29-O32)	σ (N29-O30)	0.52	0.26	0.031
LP(2)O30	σ (N29-O32)	26.03	0.46	0.099					

- Novel 1-ethylpiperazine-1,4-diium bis(nitrate) compound was synthesized.
- Optimized geometry was computed using DFT method.
- **1EPBN** was characterized by single crystal DRX.
- Charge transfer interactions were analyzed by AIM, RDG and HS analysis.
- Molecular docking studies confirmed the inhibitory activity of **1EPBN**.

Declaration of interests

☒The authors declare that they have no known competing financial interests or personal relationships that could have appeared to influence the work reported in this paper.

☐The authors declare the following financial interests/personal relationships which may be considered as potential competing interests: